# Chapter 7 – LABORATORY EXPERIMENTAL ACTIVITIES

## 7.1 GENERAL

A number of experiments were performed in order to select suitable sensors/systems for the PILASTER range, optimising operational and test/training activities with the systems in service (e.g., LTDs and LGWs), and developing new systems (e.g., LOAS). Some of these experiments, such as LGW seeker detection threshold determination, PILASTER sensors selection/characterisation tests and measurements of target materials reflection properties, were conveniently performed in a laboratory facility. On the other hand, further important measurements and tests were performed during appropriate field and flight test sessions.

Laboratory experimental activities performed during this program included the following:

- Determination of LGW Seekers Detection Thresholds;
- Measurements of Surface/Paints Reflection Properties (PILASTER targets);
- PILASTER Sensors Testing and Calibration;
- LOAS Laser System Testing; and
- Test of protection filters and eye-wears (cinetheodolites, ground crew and aircrew).

This chapter describes the laboratory experimental activities carried out during the program. Particularly, the test aims, specific test methods (instrumentation requirements, details of measures performed, etc.) and test results, are discussed in the following sections.

## 7.2 LGW SEEKER DETECTION THRESHOLD

The primary aim of this experiment was to determine the Minimum Detectable Power Density (MDPD) of a real LGW seeker. The secondary aim was to develop a test method valid for any LGW seeker system. For classification reasons, the name of the tested LGW seeker is omitted. With the available instrumentation, seeker detection threshold determination was performed in two steps:

- Seeker activation codes generation (i.e., pulse duration, PRF and train); and
- Measurement of the MDPD (pulse) based on train energy measurements.

The two steps are discussed below.

### 7.2.1 Seeker Activation Codes Generation

The STANAG 3733 titled: “Laser Pulse Repetition Frequencies (PRF) Used for Target Designation and Weapon Guidance”, defines the LGW activation codes characteristics and the related tolerances.

This activity was performed in order to check the LGW seeker functionality and properly preparing the successive power density measurements. The activity consisted in determining adequate pulse and pulse train durations, matching the instrumentation response and compatible with activation of the LGW seekers (i.e., PRF codes defined by the STANAG 3733).

In order to perform these measurements, the following instrumentation was used:

- Q-Switched Nd:YAG laser (Quantel STU-452/N);
- Nd:YAG Attenuation Filters (Quantel);

- Beam collimating optics (FIAR STU-452/N);
- Silicon Photodiode Detector (Newport Low Power Detector mod. 818-SL);
- Laser Power-meter (Newport Dual Channel Optical Meter mod. 2835); and
- Digital Oscilloscope (HP mod. 54502A and LeCroy mod. 154-B54).

Additionally, a control panel was required, including the laser remote control and the LGW seeker electrical and mechanical interfaces (necessary for guidance circuit's activation). The instrumentation set-up is shown in Figure 7-1. A detail of the target simulator is shown in Figure 7-2.

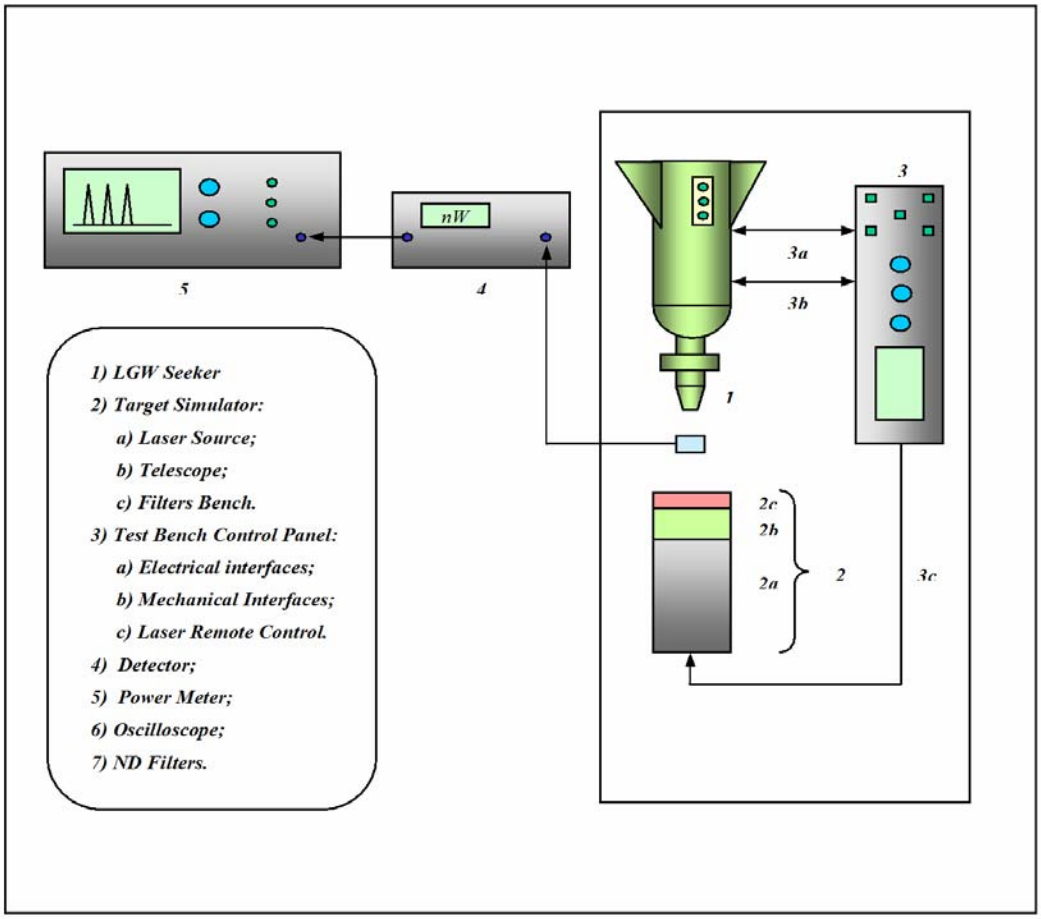


**Figure 7-1: Seeker Test Instrumentation Set-up.**

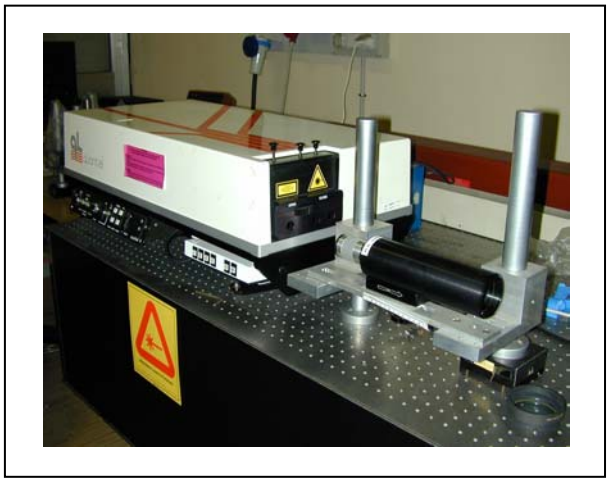

**Figure 7-2: Target Simulator.**

An initial experiment, performed with a real LGW seeker and the described instrumentation, permitted to fully characterise and reproduce some LGW activation codes (PRF according to STANAG 3733). A number of 24 activation codes were reproduced during the test (in the 10 *Hz* nominal band). After various attempts, it was verified that, for the seeker under test, the minimum pulse train duration for guidance circuits activation was about 0.5 *sec* (0.5 ± 0.1 *sec*).

The minimum number of pulses contained in each guidance activation train was variable between 5 and 6 depending on the selected code. Some oscilloscope traces are shown in the Figure 7-3 to Figure 7-5 relative to measurements performed with a specific code. Using that code, with a pulse duration of 9 *ms* and an average amplitude of 72.4 *mV* displayed on the oscilloscope (72.4 ± 2.0 *mV*), corresponding to a laser energy density of about 120 $pJ/cm^2$ (train of 19 pulses), the Full Width at Half Maximum (FWHM) was about 4.6 *ms* (4.6 ± 0.5 *ms*).

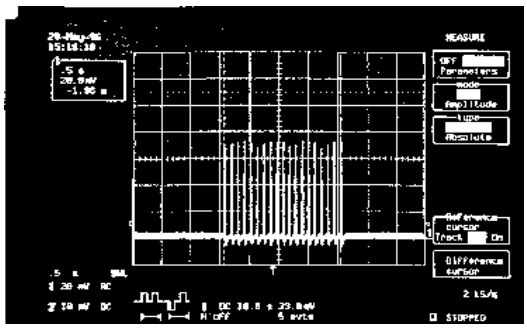

**Figure 7-3: Typical Train Profile.**

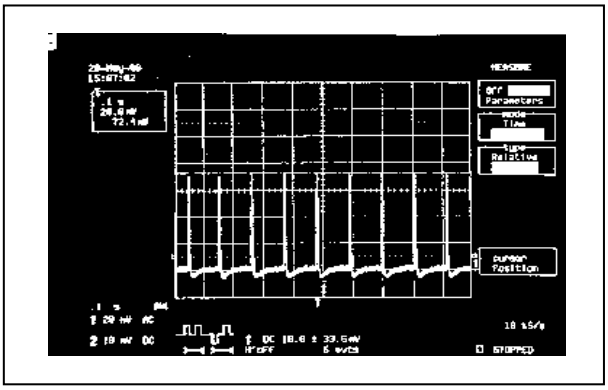

**Figure 7-4: Train Pulses Amplitude.**

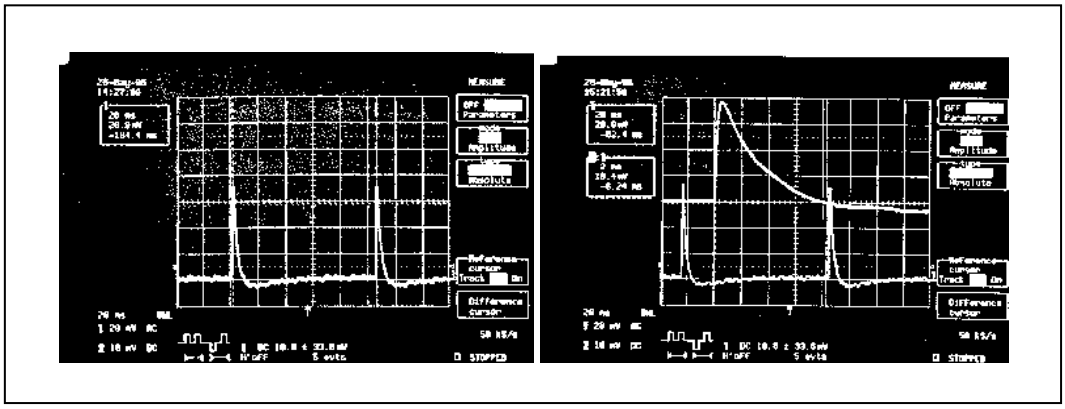

**Figure 7-5: Pulse-to-Pulse Period and Pulse Duration.**

### 7.2.2 MDPD Determination

The approach adopted for determining the Minimum Detectable Power Density (MDPD) of the seeker is described in this paragraph. The laser output energy was progressively reduced using filters of increasing neutral optical densities. Adding various suitable filters, the laser power reached a threshold value (i.e., a further small increase of attenuation prevents the seeker activation). The experimental set-up is shown in Figure 7-6.

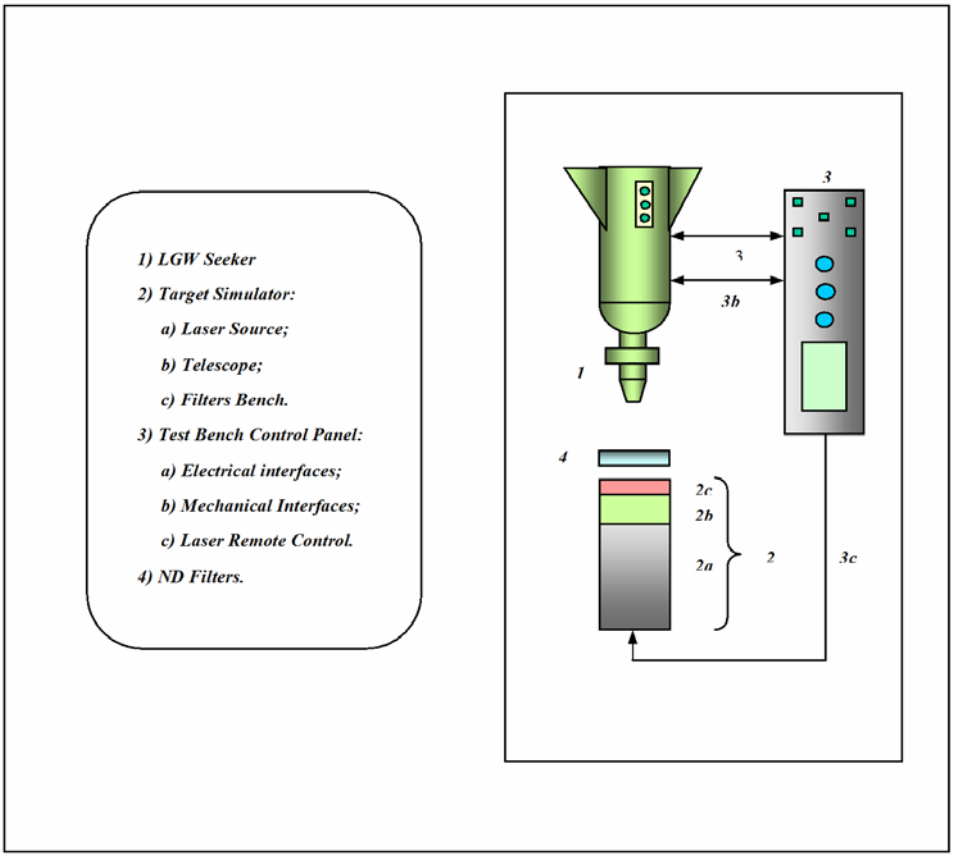


**Figure 7-6: Seeker MDPD Test Instrumentation Set-up.**

After determining the limiting condition (i.e., maximum attenuation compatible with seeker activation), the MDPD value was determined with 2 different methods:

1) By measurement, adopting the instrumentation set-up described in Figure 7-1 (with interposition of the ND filters between the detector and the target simulator), using the power meter and oscilloscope readouts; and

2) By calculation, knowing the peak power output of the target simulator and the transmittance of the ND filters.

***Method 1:*** Using the same seeker mentioned in the previous paragraph and the same activation code (i.e., pulse peak amplitude 72.4 ± 2.0 *mV*, train energy density 120 $pJ/cm^2$ , FWHM 4.6 ± 0.5 *ms* and max pulse duration 9 *ms*), an experiment was performed with the procedure described above. Using filters with an optical density greater than 0.25 ND (corresponding to a 56% transmittance), the seeker under test was not activated. With 0.25 ND, the oscilloscope measured a pulse peak amplitude of 29.9 mV. Oscilloscope traces of the original and attenuated pulse trains are shown in Figure 7-7 and Figure 7-8.

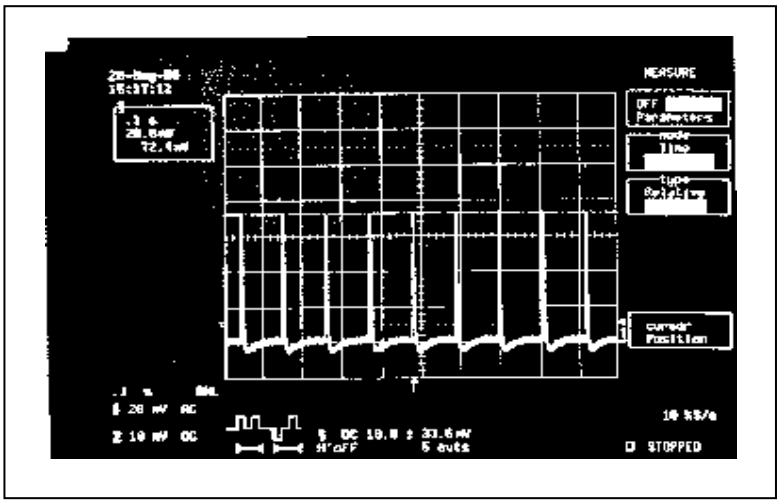


**Figure 7-7: Target Simulator Pulses Amplitude (72.4 mV).**

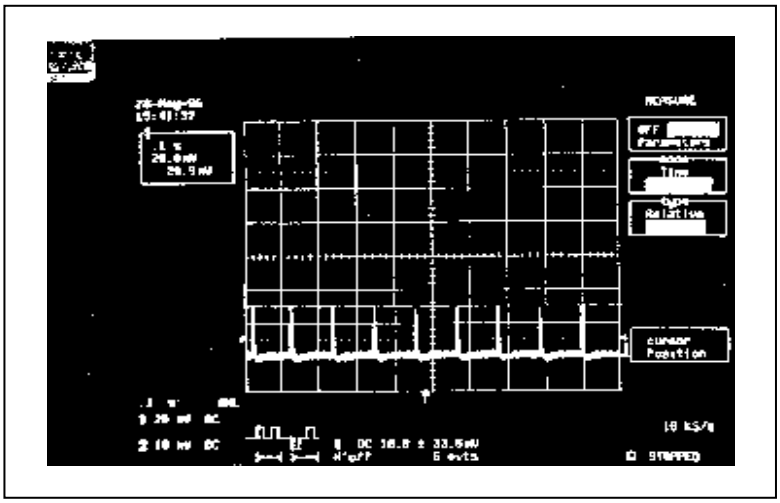

**Figure 7-8: Train Pulses Amplitude.**

Since the voltages measured by the oscilloscope were proportional to the energy measured by the power meter, the MDPD was estimated using 2 series of energy density measurements associated to the train of pulses. The results obtained with this method are given in Table 7-1.

**Table 7-1: MDPD Estimation (Method 1)**

| | | |
|---|---|---|
| ***Measurement Series*** | ***1*** | *57.8 48.0 54.0 47.0 48.0 47.5 49.0 50.0 49.0 47.0 44.0* |
| | ***2*** | *54.0 54.0 54.0 48.0 47.0 51.0 49.0 49.0 45.0 45.0 45.0* |
| ***Energy Densities*** | | *Train (avg):* $E_T \cong 50$ ***pJ/cm²***<br>*Pulse:* $E_P \cong 2.6$ ***pJ/cm²*** |
| ***Pulse Power Density Hypothesis (a): the pulse is assumed rectangular*** | | $W_P \cong 2.6$ *pJ/cm²* / *9 ms* $\cong 2.9 \times 10^{-10}$ ***W/cm²*** |
| ***Pulse Power Density Hypothesis (b): the pulse is assumed triangular (semi-base = FWHM)*** | | $W_P \cong 2.6$ *pJ/cm²* / *4.6 ms* $\cong 5.7 \times 10^{-10}$ ***W/cm²*** |
| ***MDPD (pulse)*** | | $2.9\ \mu W/m^2 < MDPD < 5.7\ \mu W/m^2$ |

***Method 2:*** Using filters with an optical density greater than 0.25 ND, the seeker under test was not activated. Therefore, since this limiting condition corresponded to a 56% transmittance, the MDPD value was calculated using the target simulator known power density output (8 μW/m²) as follows:

$$MDPD = 8\,\mu W/m^2 \times 0.56 \cong 4.5\,\mu W/m^2 \tag{7.1}$$

## 7.3 LASER BEAM PROFILING

Laser Beam Profiling (LBP) in a laboratory facility was an additional requirement for the PILASTER program, as it was necessary in order to determine the output characteristics of the laser systems under test, before performing experimental measurements at the range. Furthermore, some experiments performed during the program (i.e., laboratory tests, field trials and flight test activities) had to be carried out in well defined and repeatable conditions, in order to detect errors affecting the measurements, thus defining the validity and applicability of the results. Also in these cases LBP was used.

Therefore, various CCD cameras and suitable software packages for beam profiling were examined, in order to select a combination suitable for matching the PILASTER test requirements. The features common to all software packages included:

- Intensity distribution analysis;
- Gaussian fit analysis;
- Image, capture, store, and playback of 2-D and 3-D intensity plots; and
- Printing of text and pictures.

Typical examples of a program outputs are shown in Figure 7-9.

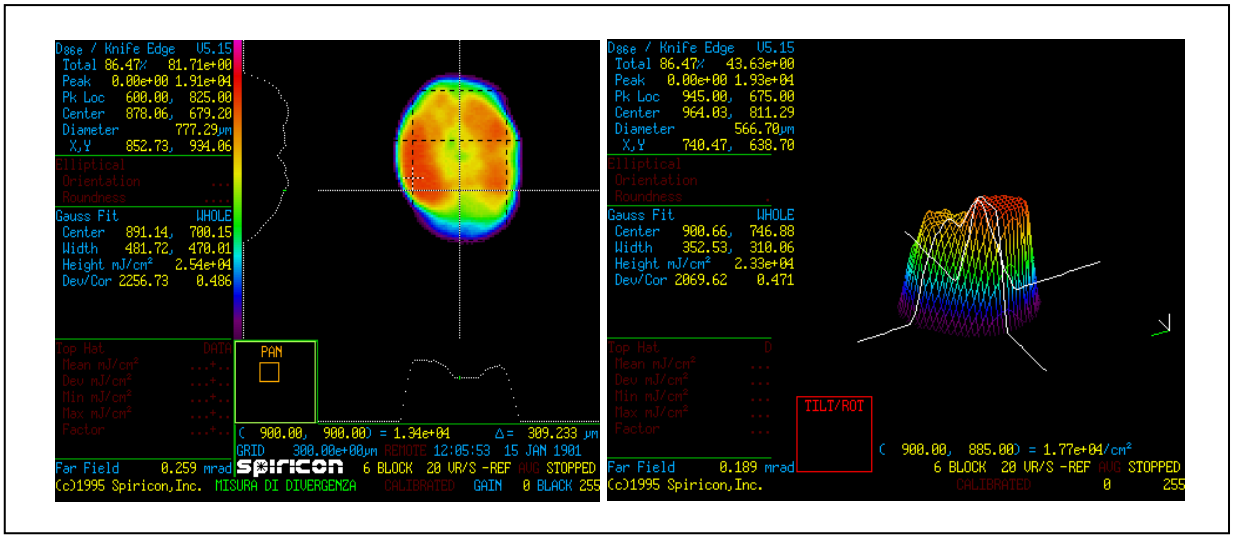


**Figure 7-9: Spiricon™ (Ophir Optronics Ltd.) 2-D and 3-D Display Format.**

In order to match the various PILASTER requirements, the laser beam profiler should be able to analyse both continuous wave (CW) and pulsed lasers, and detect a wide range of different signals (power levels, PRFs, pulse durations, etc.). The main technologies available today for laser beam diagnostics are:

- Spatial cameras as the beam characterisation system.
- Moving mechanical slit or knife edges to scan across the incoming beam.

The main advantage of the mechanical scanning devices over a camera type laser beam profiler is the large dynamic range that allows accurate measurements of beams with both high and low intensities. On the other hand, camera type laser beam profilers are excellent for fast and detailed analysis of laser beam intensity profiles, but are limited in their accuracy due to a relatively low dynamic range.

However, to overcome the limited dynamic range of a camera type beam profiler and accurately measure faint laser beam structures, it is possible to sample the beam several times, each measurement being performed at a different attenuation or electronic shutter speed.

Although initial experiments were carried out with the Spiricon™ CCD profiler, the BeamStar™ profiler (by Duma Optronics Ltd.) was finally selected for the PILASTER program. Various types of cameras can be used with this software. The standard camera, supplied with the beam profiler software (Figure 7-10), is a Monochrome Interline Transfer CCD ½", with an active area of 6.47 × 4.83 mm. The camera spectral response is 190 – 1100 nm and the maximum power density on filter is 50 W/cm$^2$. With this CCD camera, using electronic shuttering and ND filters, the system (with software) can capture and reply pictures and statistics from both continuous and pulsed lasers. In the first case, the maximum optical dynamic range is $2 \times 10^8$:1 (shutter speeds 1/50 to 1/10000 sec) and the maximum frame rate is 30 Hz. For pulsed lasers (1 – 100 Hz), the optical dynamic range is 256:1. For transmission of the output images (640 × 480 resolution) and data, an RS-232 standard interface is available (also available for a remote control).

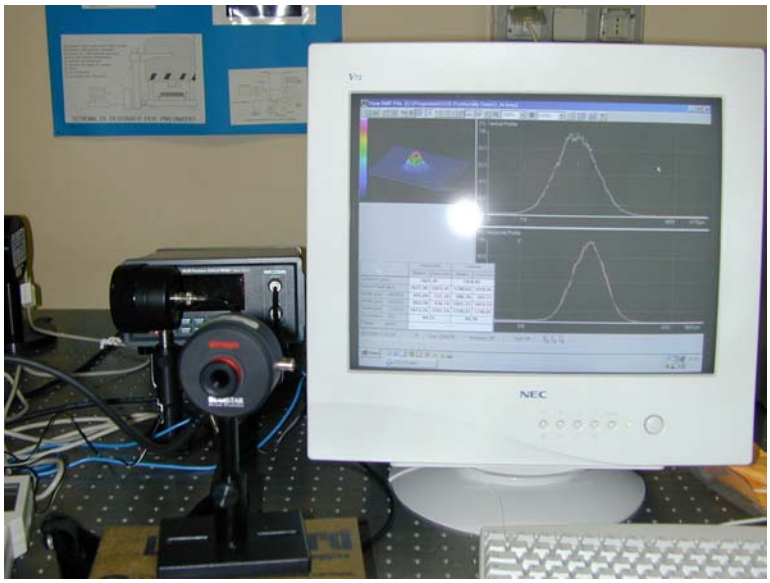


**Figure 7-10: Beamstar™ CCD Camera.**

## 7.4 SURFACE REFLECTION MEASUREMENTS

Determination of target surface reflection properties at laser wavelengths is essential for predicting realistic range performance of ground and airborne laser systems, as well as for aircraft tactics (flight profile) optimisation, test range design activities, analysis of flight/ground test data and assessment of training exercises with laser systems. In the following paragraphs, we describe the test activities performed for determining both the general reflection properties of various materials/paints in the visible and infrared portions of the spectrum (i.e., in terms of total reflectance), and the specific reflection characteristics of the PILASTER target materials at Nd:YAG laser wavelength ($\lambda$ = 1064 nm) subject to specific geometrical constraints, in terms of Bidirectional Reflectance Distribution Function (BRDF). An essential pre-requisite for both activities was the correct analysis of target materials physical properties, such as surface profile characterisation (roughness statistics, coating/painting standards, etc). LBP was also performed during BRDF measurements to ensure repeatability of the experiments.

### 7.4.1 Samples Identification and Surface Characterisation

The samples for surface scattering measurements were selected in order to allow an appropriate choice of the paints to be used for the PILASTER targets (Group-I), and also to gather useful data regarding the reflective properties of materials normally encountered in the operational use of laser systems (Group-II). The samples selected for both reflectance and BRDF measurements (i.e., candidates for construction of the PILASTER targets), were the following:

***Group-I***

a) White *Spectralon™* (*Labsphere Ltd.*);

b) White Refractive Road Paint (GEN-M-P0017);

c) White Building Paint (*Baldini S.p.A.* n° 345.998);

d) Diffusive Black Paint (*Nextel™* 97B/3W – AER-M-P039e);

e) Diffusive White Paint (*Nextel*™ 3B/97W – AER-M-P039a);

f) White Non refractive Road Paint (GEN-M-P0016);

g) Dark Grey Paint (AER-M-G039f);

h) Light Green Paint (AER-M-H067d); and

i) Dark Green Paint (AER-M-H074e).

The sample of Spectralon™ (whose BRDF characteristics were provided by the manufacturer) also served to test the BRDF measurement instrumentation set-up.

The materials selected for reflectance measurements only ($\lambda$ = 400 – 1200 nm) were the following:

***Group-II***

a) IR Grey Paint n° 1 (AER-M-G056);

b) IR Grey Paint n° 2 (FS 36280);

c) Concrete n° 1 – Runway;

d) Concrete n° 2 – Shelter;

e) Airport Parking Area Material;

f) Asphalt n° 1 – Runway; and

g) Asphalt n° 2 – Road Material.

All paint samples were prepared using 2 × 2 inches polished aluminium plates. Before performing BRDF measurements, the rms surface roughness ($\sigma$) and slope ($s$) of the Group-I samples was measured using a surface profilometer (*Hommer Tester* T1000) which measured the surface roughness every 0.25 μm along a 15 mm scan. The rms roughness of the samples ranged from 0.42 μm to 16.87 μm. The results of the measurements are listed in Table 7-2.

**Table 7-2: Surface Characterisation for BRDF Measurements**

| Sample | rms Roughness ($\sigma$) | rms Slope ($s$) |
|---|---|---|
| a | 0.47 μm | 11.4° |
| b | 6.88 μm | 23.6° |
| c | 19.96 μm | 22.4° |
| d | 4.80 μm | 22.3° |
| e | 4.41 μm | 24.3° |
| f | 1.76 μm | 20.5° |
| g | 1.52 μm | 18.1° |
| h | 0.60 μm | 11.7° |
| i | 0.42 μm | 13.5° |

### 7.4.2 Reflectance Measurements

As a first step into the analysis of the samples reflection properties, reflectance measurements were performed in the visible and near infra-red ($\lambda$ = 400 – 1200 nm). The measurements were performed with the integrating-sphere spectrophotometer Perkin-Elmer mod. 'Lambda 19'. The results obtained for the two groups of samples are presented in Figure 7-11 and Figure 7-12.

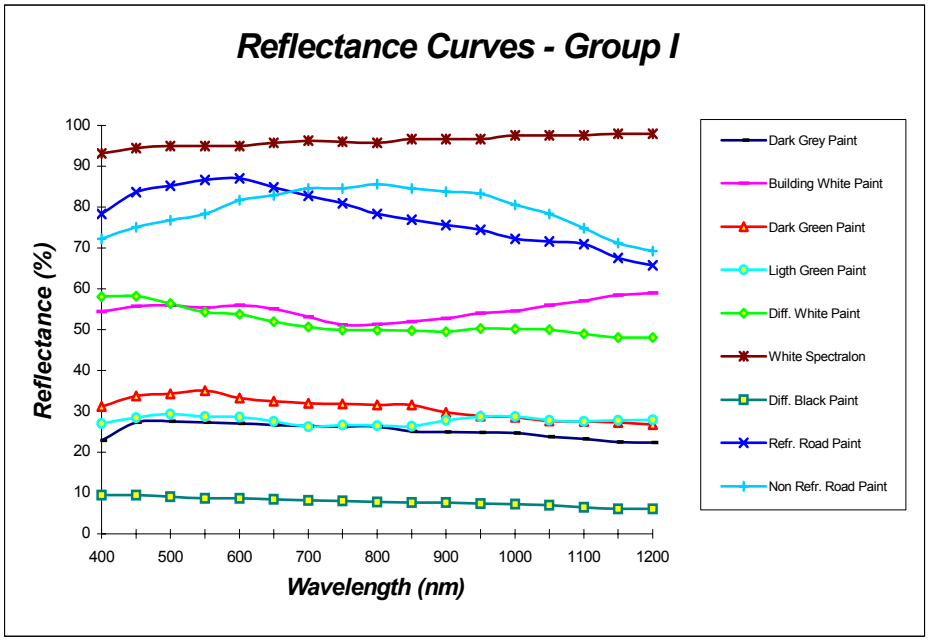


**Figure 7-11: Group-I Reflectance Measurements Results.**

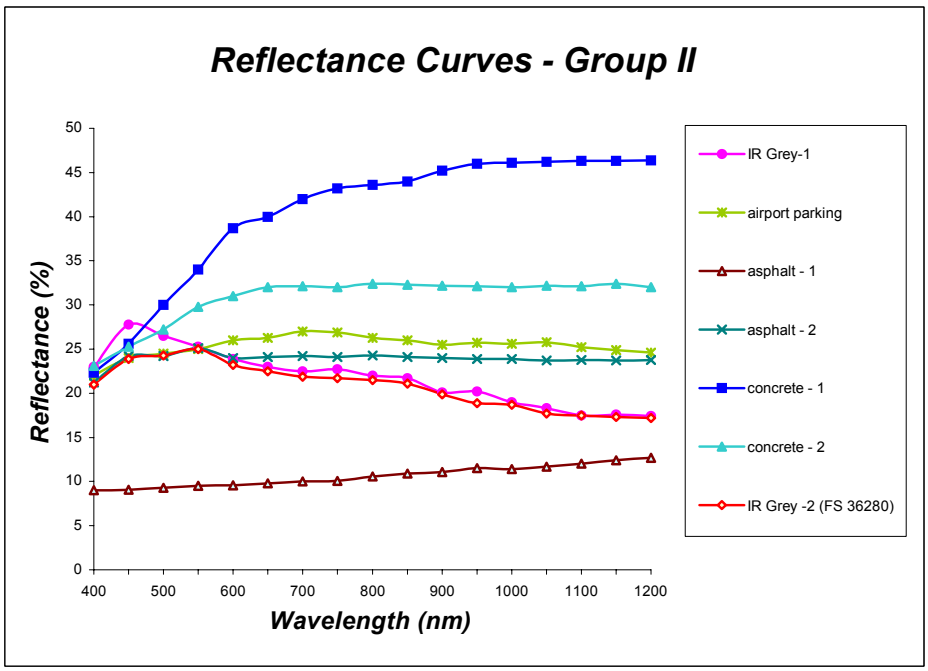


**Figure 7-12: Group-II Reflectance Measurements Results.**

### 7.4.3 BRDF Measurements

The Bidirectional Reflectance Distribution Function (BRDF) is defined as the ratio of the radiance of a sample to the irradiance upon that sample, for a given direction of incidence and direction of scatter. For BRDF measurements with the Group-I samples (i.e., PILASTER targets candidate paints and materials), a Laser Scatter-meter (LSM) was built. To briefly summarise the fundamental concepts involved, necessary to describe the LSM experimental arrangement, we refer to the LSM beam coordinate system illustrated in Figure 7-13.

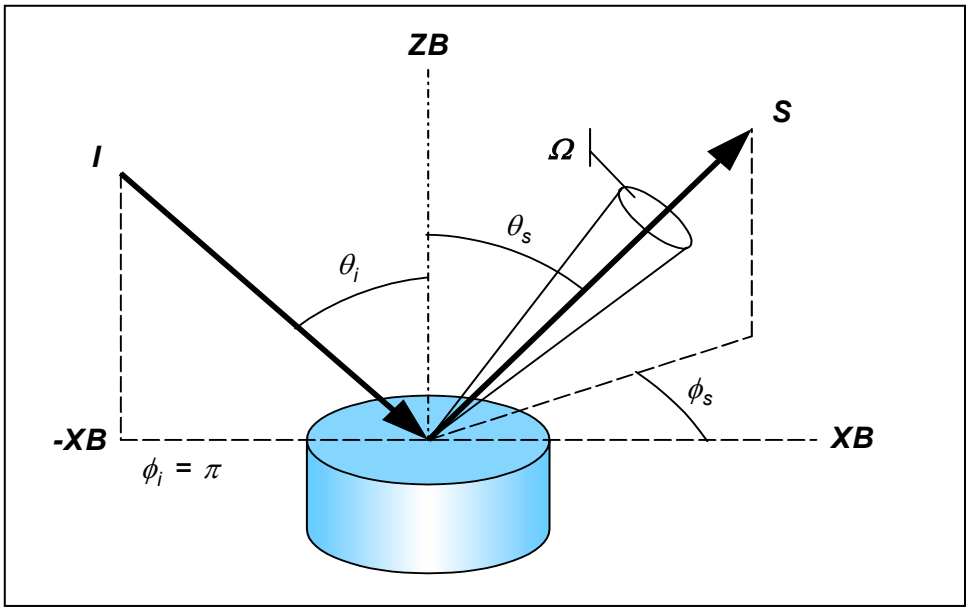


**Figure 7-13: LSM Beam Coordinate System.**

The origin of the beam coordinate system is the point at which the central ray of the incident radiation ($I$) strikes the sample surface. The $ZB$ axis is normal to the sample surface, and the $XB$ axis lies in the plane defined by $ZB$ and $I$. The incident direction is specified by two angles: the angle of incidence ($\theta_i$), and the incident azimuth angle ($\phi_i$), where $\phi_i = \pi$ by definition. Similarly, the scatter direction is specified by the scatter angle ($\theta_s$), and the scatter azimuth angle ($\phi_s$). In order to measure BRDF, a LSM should allow the sample to be illuminated with a collimated laser beam from a range of incident directions. Furthermore, a receiver, subtending a solid angle $\Omega$ and viewing the entire illuminated area, should be positioned at a range of scatter directions. For any given LSM configuration, an average sample irradiance ($E_e$) is calculated from the power $P_i$ incident on the sample and the illuminated area $A$. An average sample radiance $L_e$ is calculated from the power $P_s$ collected by the receiver, the receiver solid-angle, and the area of illumination. Therefore, the sample BRDF is calculated as the ratio of these two quantities:

$$BRDF = \frac{L_e}{E_e} = \frac{\left(P_s / \Omega A \cos\theta_s\right)}{\left(P_i / A\right)} = \frac{P_s}{P_i \Omega \cos\theta_s} \qquad \left[sr^{-1}\right] \tag{7.2}$$

Alternatively, the relative radiance of the sample may be measured versus that of a standard whose BRDF is known for the bi-directional geometry in question. The sample BRDF may then be calculated by multiplying the resulting ratio by the known BRDF of the standard.

Our LSM limits the collection of BRDF data to receiver positions in the plane of incidence, which is defined by the central ray of the incident flux and the sample normal. This is referred to as “in-plane” data

(data collected with receiver positions confined to the plane perpendicular to the plane of incidence, and containing the sample normal, is referred to as "cross-plane" data).

BRDF, with its units of inverse steradians, appears as a fairly abstract quantity. The BRDF of a given sample is closely related to a more concrete quantity, however, its bi-directional reflectance factor. This is defined as the ratio of the flux scattered in a given direction by the sample, to that which would be scattered in that direction by the perfect reflecting diffuser, under identical conditions of illumination. The relation between BRDF ($B$) and bi-directional reflectance factor ($R$) is expressed by:

$$R(\theta_i, \phi_i, \theta_s, \phi_s) = \pi B(\theta_i, \phi_i, \theta_s, \phi_s) \tag{7.3}$$

It is important to observe that the BRDF of a perfectly diffuse (Lambertian) sample would be constant for all bi-directional geometries. However, the power collected by the receiver ($P_s$) is strongly dependent on the scatter angle ($\theta_s$), and becomes very small as $\theta_s$ approaches $\pi/2$. For this reason, we should expect that the effects of noise, and other sources of measurement error, become much more pronounced at large scatter angles.

Both the polarization state of the incident flux and the polarization bias of the receiver may be important variables in BRDF measurements. Many scattering materials significantly depolarise incident flux, while other materials selectively absorb flux with a certain polarization. A complete characterization of sample scattering also requires evaluation of these polarization effects. The experimental arrangement of the LSM is shown in Figure 7-14.

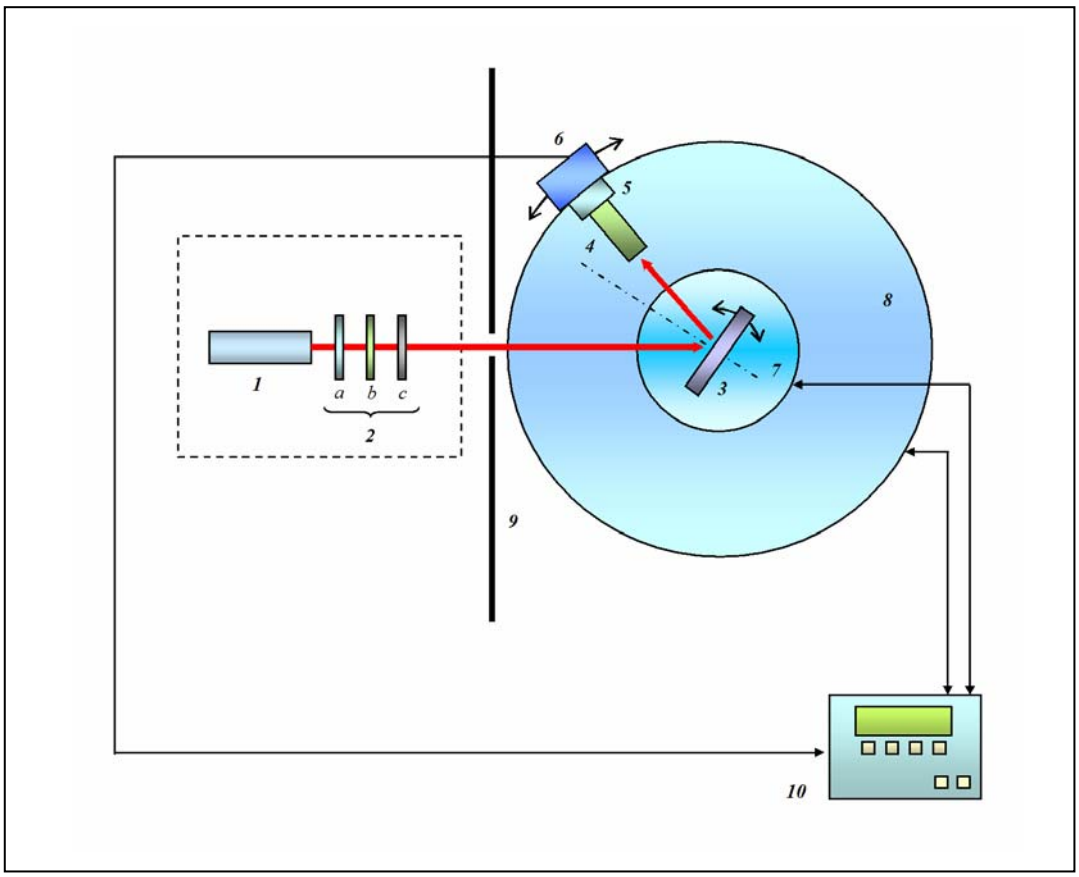


**Figure 7-14: Laser Scatter-Meter Experimental Arrangement.**

The LSM was composed by three main parts: (A) the laser unit (including the laser source and the intensity/ polarization control units), (B) the target turn-table unit (allowing orientation of the target sample), (C) the detection unit, mounted on a second turn-table (including the collimator, the polarizing filter and the detector), and (D) the measurements unit, including the energy/power meter and a motion control unit for automatic (continuous) data acquisition, both connected to a PC for data monitoring and recording. Particularly, with reference to Figure 7-14, the LSM employed the following components:

1) Laser source.
2) Intensity and polarization control:
   a) ND filters;
   b) Linear polarizer; and
   c) Retardation plates.
3) Sample.
4) Collimator, 5) Polarising filter (analyser) and 6) Detector.
7) Sample turn-table and 8) Receiver turn-table.
9) Light shield.
10) Energy/power meter, motion control unit and computer.

The BRDF measurements were performed at a wavelength of 1064 nm (Nd:YAG laser). Particularly, the BRDF of Group-I samples was determined. Before performing BRDF measurements, the characteristics of the Nd:YAG laser beam incident on the sample surface were determined using the BeamStar™ CCD profiler. The parameters relative to the Gaussian fit of the horizontal and vertical cross-sections of the beam produced by a single laser pulse are shown in Figure 7-15. Particularly, in this case, a difference is evidenced between the shapes of the horizontal and vertical cross-sections (also due to the distortions introduced by the LSM optical circuit), leading to a correlation with the Gaussian fit of about 80% in both cases. With laser sequences of up to 10 seconds in duration and PRF up to 20 Hz, it was also found that the stability of the beam shape (i.e., correlation with the Gaussian fit) was always within a limit of 73%.

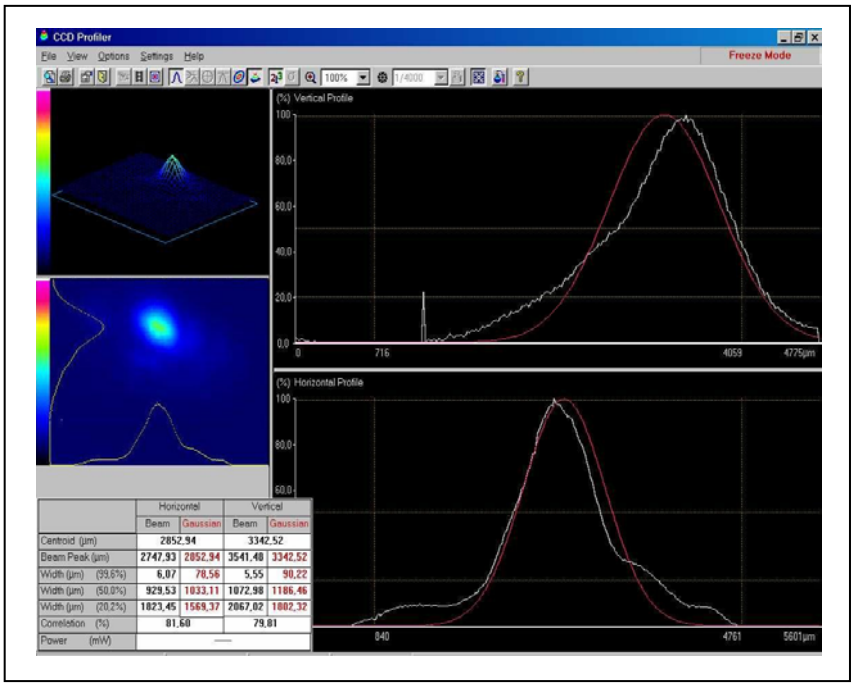


**Figure 7-15: Nd:YAG Laser Beam Profile for BRDF Measurements.**

All BRDF measurements were performed with linearly polarised illumination, with the direction of polarization parallel (*P*) to the plane of incidence. In selected cases (samples d and e), the receiver was also polarised, with bias parallel (*P*) or perpendicular (*S*) to the plane of incidence. In this case, for a material which does not affect the polarization of the incident flux, the observed BRDF for the cross-polarized configuration (*PS*) would be zero. On the other hand, for a perfect depolarising sample, the BRDF values would be identical for both (*PP*) and (*PS*) measurement configurations.

The results of the BRDF measurements are reported below in the Figure 7-16 to Figure 7-24. Particularly, the BRDF relative to all samples for three different laser incidence angles ($\psi$ = 0°, 30°, 45° and 60°) are reported. Furthermore, the BRDF variations with receiver polarization parallel (*P*) and perpendicular (*S*) to the plane of incidence (with $\psi$ = 0° and 45°) are reported for the two paints that, after the initial reflectance and BRDF measurements, were identified as the best candidates for the PILASTER targets (samples d and e).

**a. White Spectralon™**

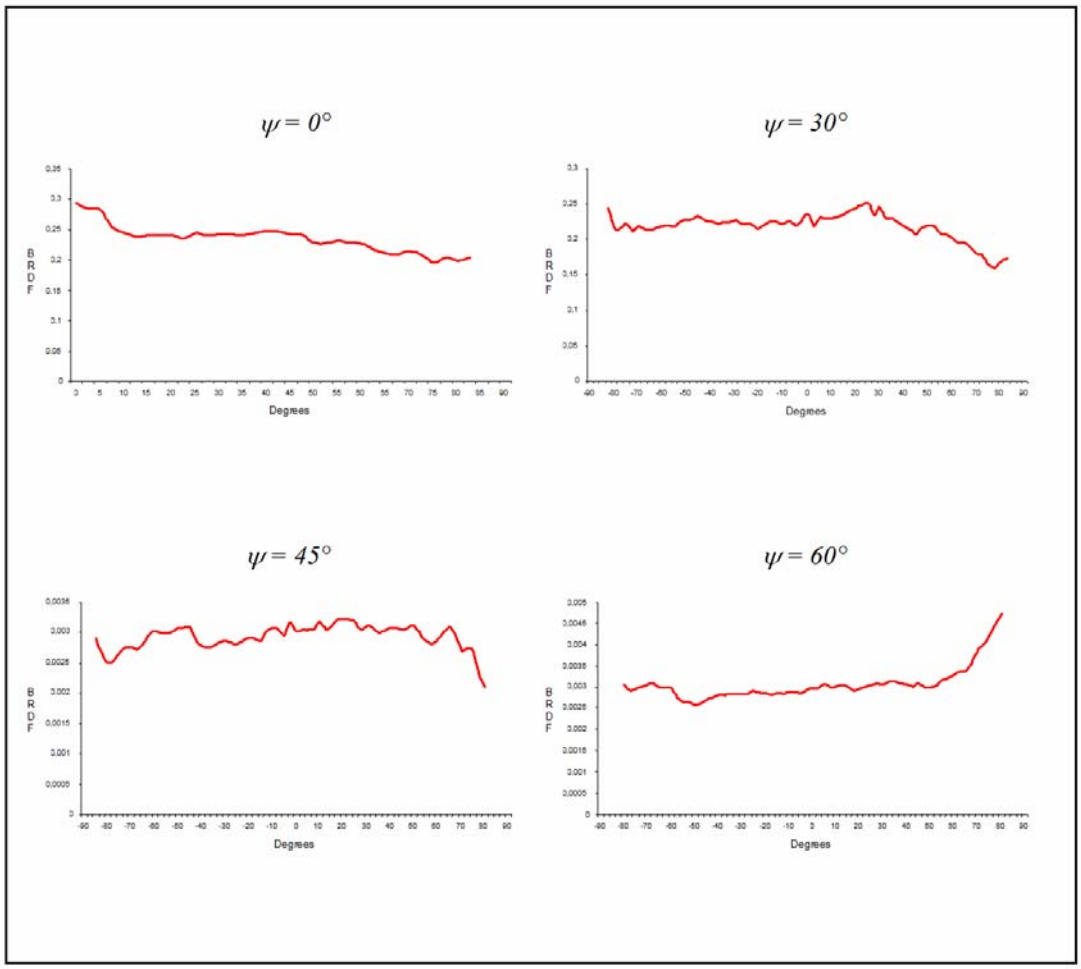


**Figure 7-16: BRDF for White Spectralon.**

## b. White Refractive Road Paint

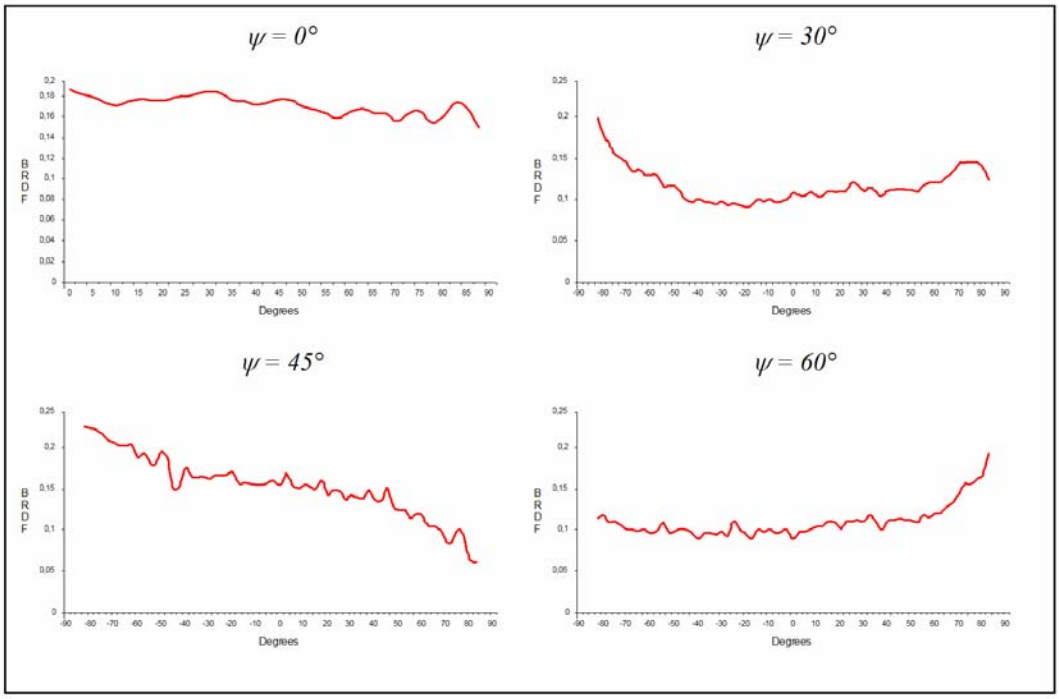


**Figure 7-17: BRDF for White Refractive Road Paint.**

## c. Building White Paint

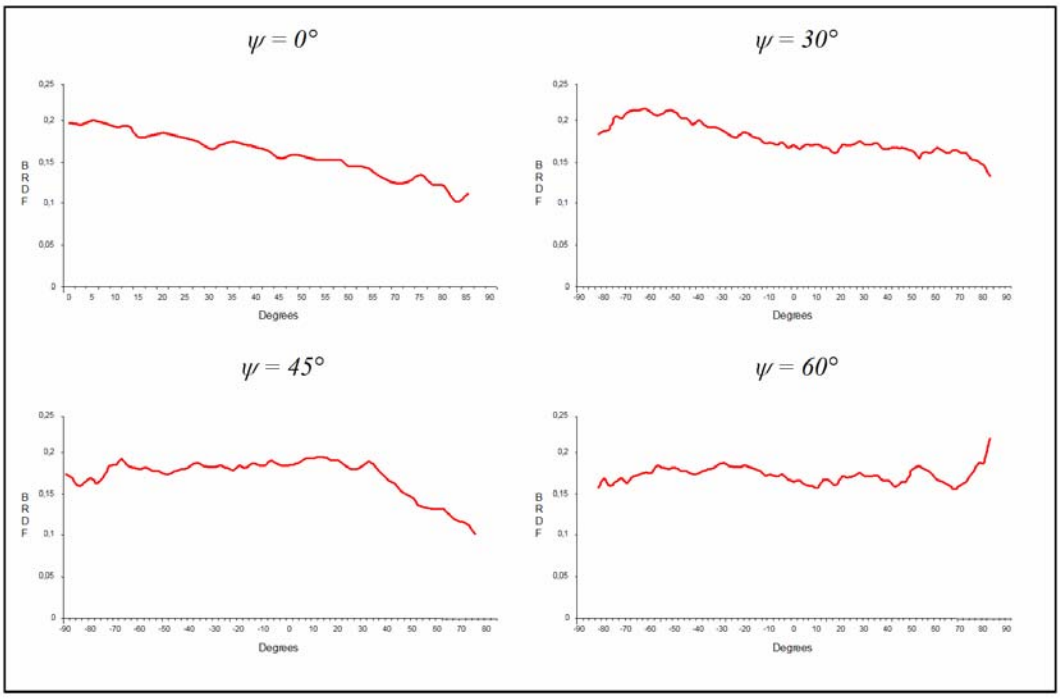


**Figure 7-18: BRDF for White Building Paint.**

## d. Diffusive Black Paint

**Figure 7-19: BRDF for Highly Diffusive Black Paint.**

## e. Diffusive White Paint

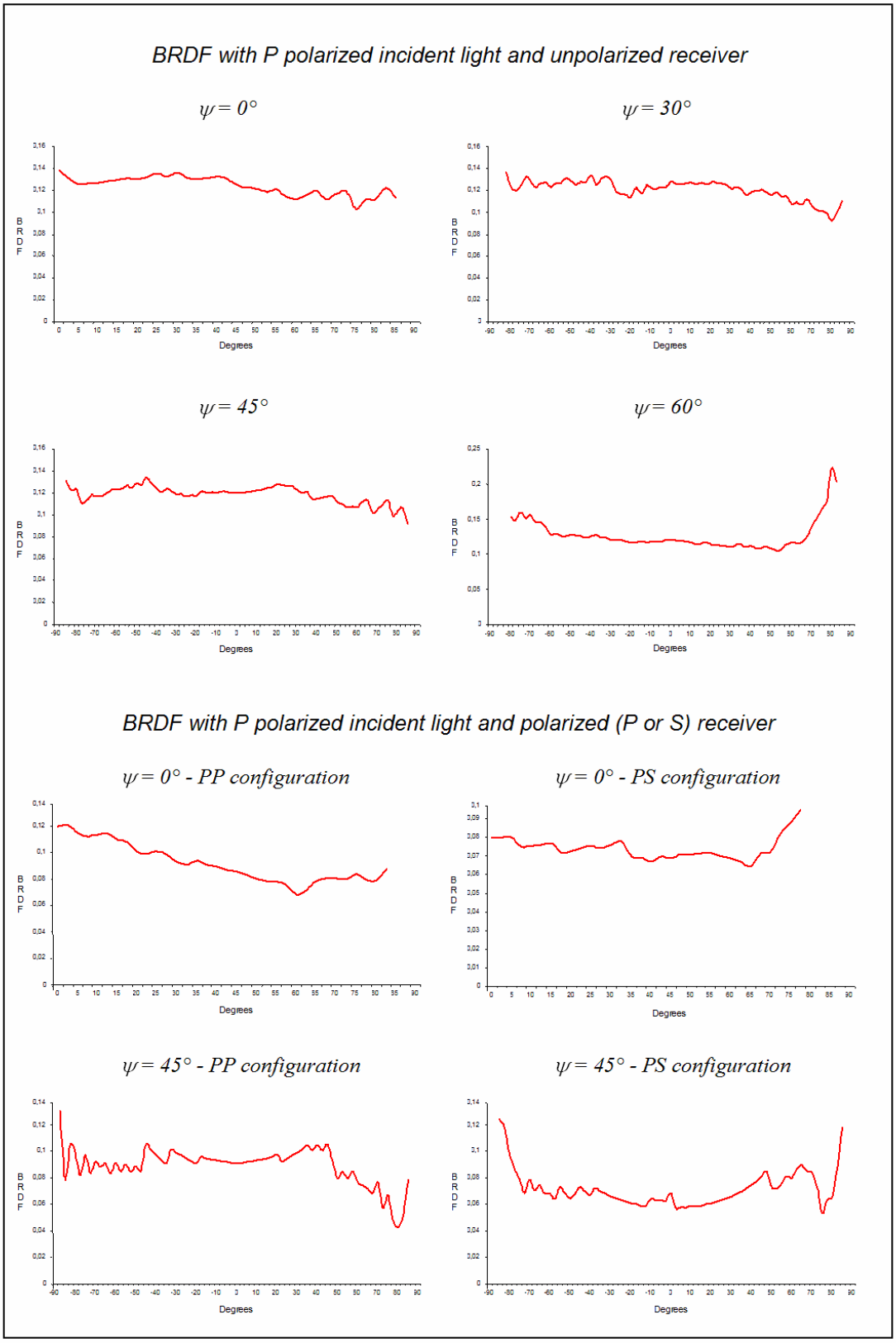


**Figure 7-20: BRDF for Highly Diffusive White Paint.**

## f. White Non-Refractive Road Paint

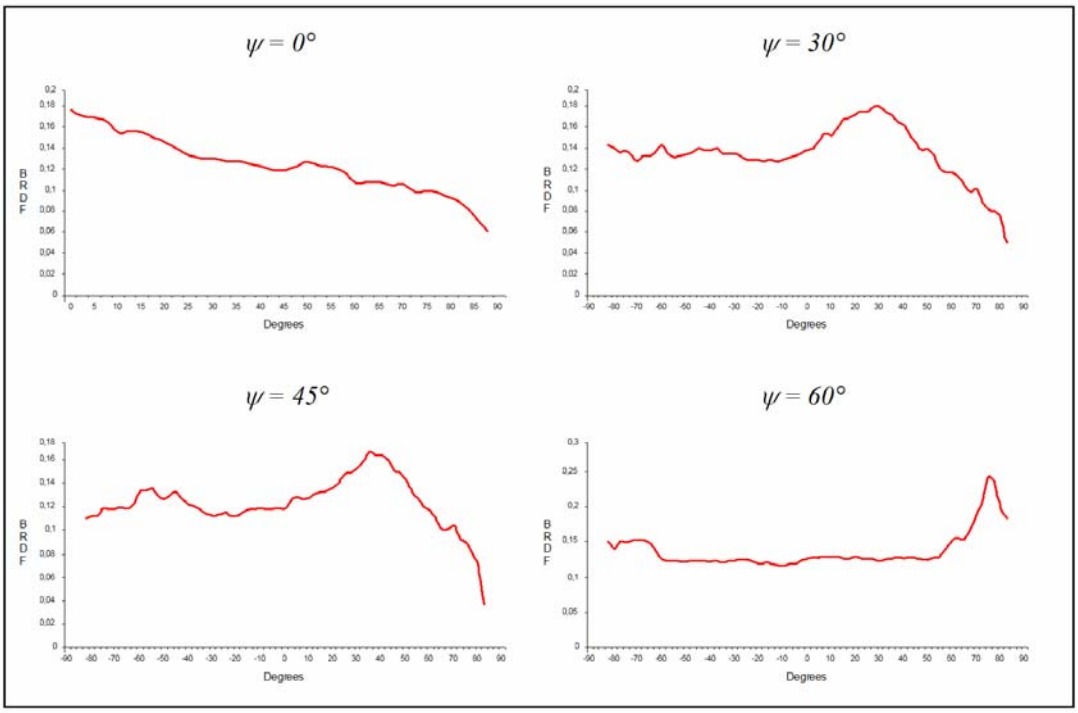


**Figure 7-21: BRDF for White Non-Refractive Road Paint.**

## g. Dark Grey Paint

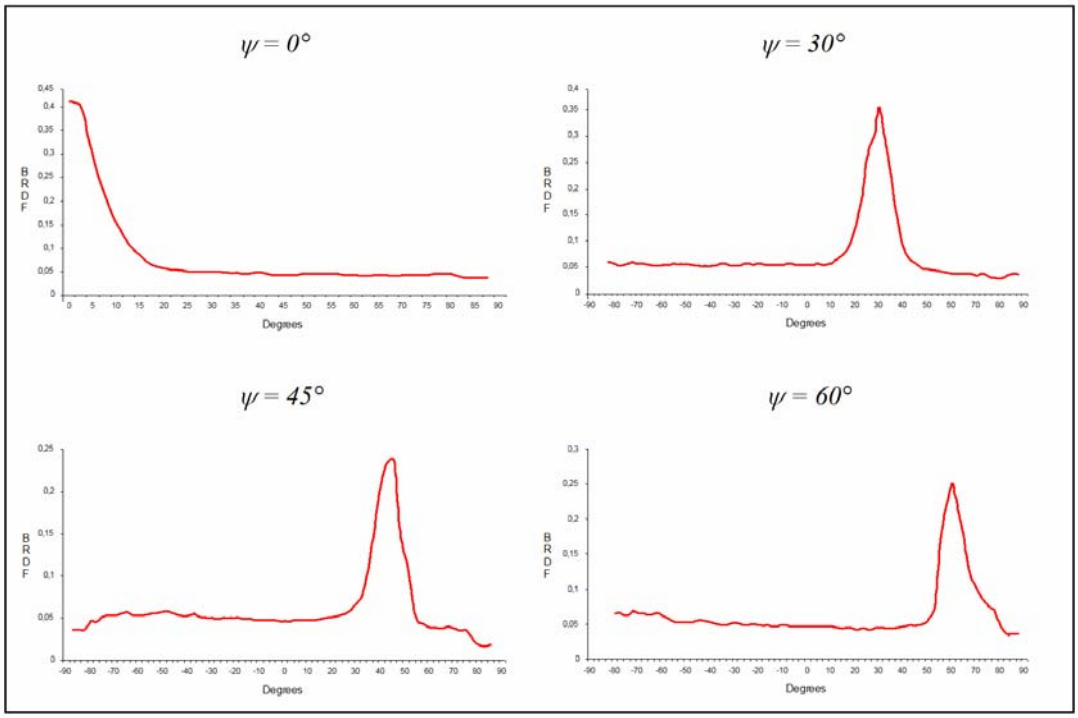


**Figure 7-22: BRDF for Dark Grey Paint.**

## h. Light Green Paint

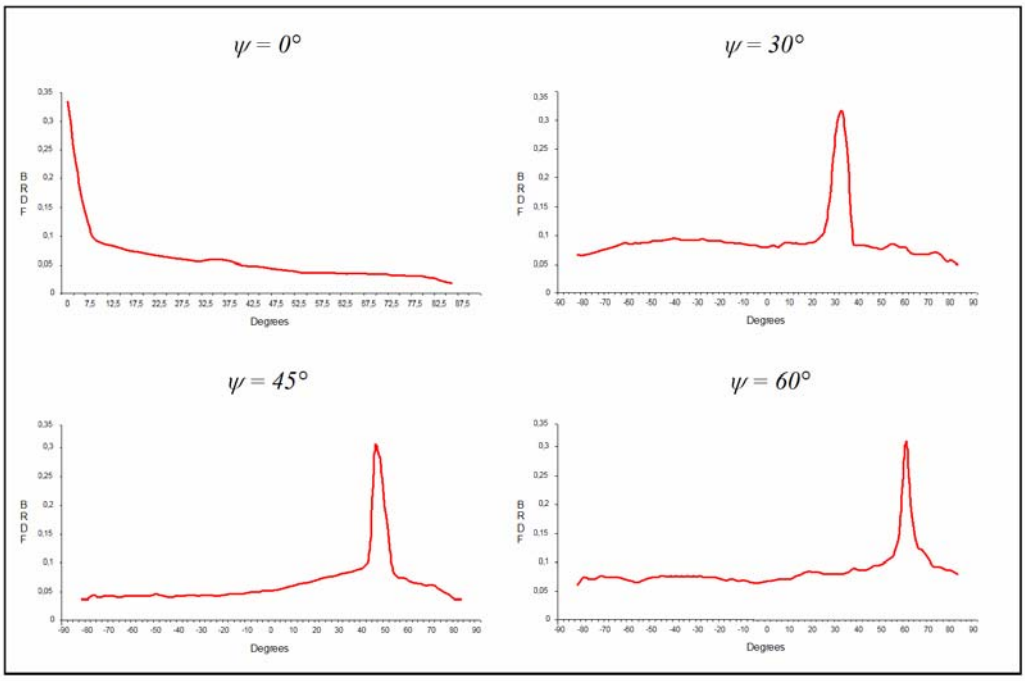


**Figure 7-23: BRDF for Light Green Paint.**

## i. Dark Green Paint

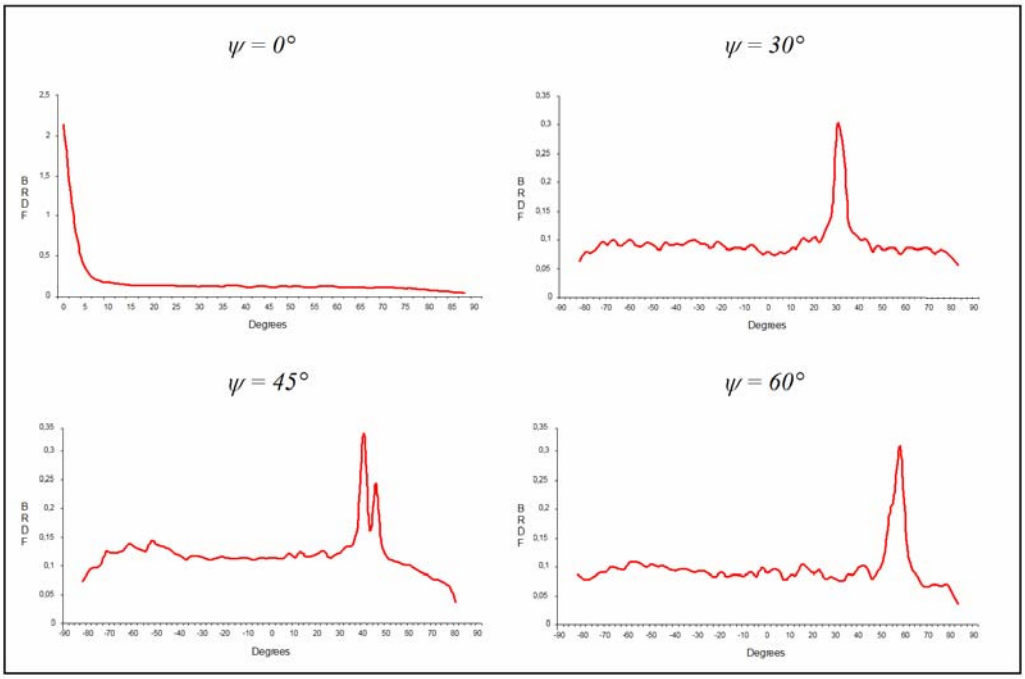


**Figure 7-24: BRDF for Dark Green Paint.**

Due to their excellent contrast in the visible and their good *Lambertian* characteristics, the Diffusive Black Paint AER-M-P039e (sample d) and the Diffusive White Paint AER-M-P039a (sample e), were selected for the PILASTER permanent target (FXDT) panels. Although these paints were technically adequate also for the PILASTER FRCT modular target (i.e., destroyable target for real weapon deliveries), they were not used for this application due to their very high cost. In this case, a combination of the Dark Grey Paint AER-M-G039f (sample g) with either the White Non refractive Road Paint GEN-M-P0016 (sample f), or the White Refractive Road Paint GEN-M-P0017 (sample b), was considered acceptable. It must be underlined that all these paints (samples b, d, e, f and g) are produced for employment by the Italian military forces, and their reflectance characteristics are claimed to remain constant in a wide range of environmental/weather conditions and due to aging. The use of the low cost White Building Paint *Baldini* n° 345.998 (sample c), was suggested only when laser spot measurements on the PILASTER targets were not required (being the only non military product, the characteristics of this paint may vary significantly due to aging or other factors).

## 7.5 PILASTER SYSTEMS TESTING

Laboratory experimental activities also included initial tests for selection of the systems/sensors candidate for the PILASTER Program. These activities included:

- Near Infrared Cameras (NIR) Testing;
- Modified Laser Warning Receiver (LWR) System Testing; and
- Power/Energy Meter and Detectors Testing.

Test methods and results are described in the following paragraphs.

### 7.5.1 NIR Cameras Testing

Two NIR cameras based on Focal Plane Array (FPA) sensors were tested for use in the PILASTER program, these are:

- the MERLIN™ NIR camera; and
- the PHOENIX™ NIR camera;

both produced by the Indigo Systems Corporation (USA). Both NIR cameras had a spectral band 0.9 – 1.7 µm, and employed Indium Gallium Arsenide (InGaAs) detectors. In both cases, the array format was 320 H × 256 V and the detector size was 30 microns. Furthermore, optics with different focal lengths and FOV/IFOV were available (e.g., 25 and 50 mm focal lengths with FOV/IFOV of 22° × 16°/1.3 mrad and 11° × 8°/0.6 mrad respectively). Both cameras were equipped with real-time imaging electronics, remote controls, and NTSC/PAL video outputs. The PHOENIX™ camera was also equipped with a high-speed digital acquisition system, composed of a rack mount, high speed Pentium™ processor, a camera interface/ sync board and Bit-Flow frame grabber. It captured the full bandwidth of digital video from the camera (40 MHz) and provided pseudo real-time VGA video for aiming and focusing the camera.

The aim of the laboratory test activity was to verify the performance of the PHOENIX and MERLIN NIR Cameras (together with the relative Data Acquisition Systems) in the presence of laser spots generated by very short laser pulses (PD < 20 nsec), with PRF, energy levels and spot characteristics compatible with the PILASTER requirements. With reference to the test setup shown in Figure 7-25, the following systems and instrumentation were used for the experiments:

- PHOENIX and MERLIN NIR Cameras (1);
- PC based Data Acquisition Systems (2) with IMAGE-PRO PLUS 4.1 Software;
- Laboratory Target 3.0 × 1.5 m (3);

- Q-Switched Nd:YAG laser (4);
- Nd:YAG Attenuation Filters (5);
- Beam Splitter (6) and Mirror (7);
- Beam Expanding Optics for Narrow (8) and Wide Laser Beams (9); and
- Aberration Filter (10).

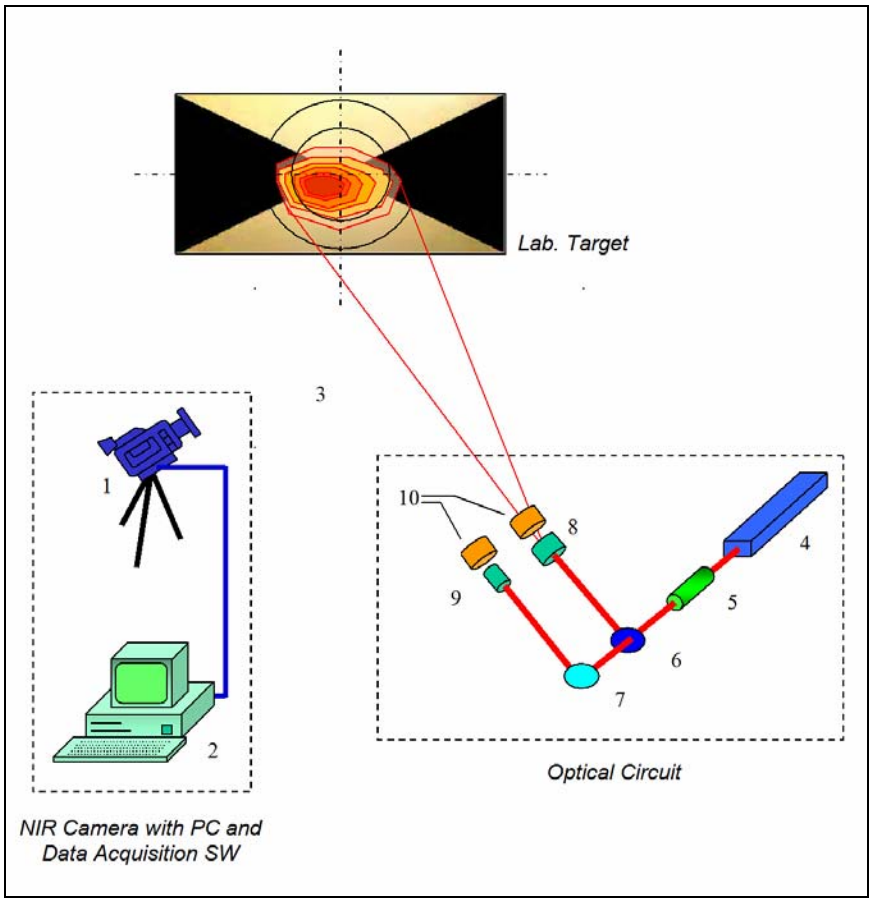


**Figure 7-25: NIR Cameras Test Instrumentation Setup.**

The 3.0 × 1.5 m target, painted in back and white with paints of considerably different reflectance at 1064 nm (i.e., 7% and 50% respectively), was located at a distance of about 5 m from the beam expanding optics ($\Phi_{wide}$ = 50 mrad and $\Phi_{narrow}$ = 2 mrad). With this geometry, the effective spot diameters were about 50 cm and 2 cm. The PHOENIX/MERLIN NIR Cameras, equipped with suitable optics (in order to see the entire target) and connected to the Data Acquisition PC, was also located at a distance of about 5 metres from the target. An Aberration Filter (AF) was also used at the expanding optics output to generate highly distorted laser spot profiles on the target (with similar characteristics to the spots expected to be encountered in the future operational use of the cameras at the PILASTER).

During the test, the different requirements associated with the intended use of the two cameras were taken into account, setting appropriate integration times for data acquisition in order to obtain:

- Post-processing data analysis (i.e., geometry, energy distribution, time analysis), for the maximum number of pulses (spots) in a sequence, for the PHOENIX NIR camera; and
- Real-time visualization of the spot sequence, in the case of the MERLIN NIR camera.

For both NIR cameras, an important requirement was to minimise the memory required for frames recording, maximising at the same time the performances of the cameras with and without synchronisation of spot data acquisition with laser signal transmission (i.e., number of useful frames for the PHOENIX NIR camera and quality of the real-time displayed image for the MERLIN NIR camera). Therefore, it was first of all necessary to find adequate Frame Frequencies ($f_F$) of the NIR cameras according to the specific application. This was done in order to maximise the number of recorded pulses in the first case (PHOENIX NIR camera) and to obtain high quality real-time sequences in the second case (MERLIN NIR camera). A number of tests were performed in order to experimentally determine the optimal $f_F$ for the two NIR cameras. A more detailed analysis for $f_F$ optimisation was performed during the ground test activities (see Chapter 8). In general, setting the $f_F$ at twice the PRF, it was empirically found to be a good compromise for the PHOENIX NIR camera, while for the MERLIN NIR camera intended application (i.e., real-time spot monitoring) a $f_F$ of 10 Hz was adequate for PRFs of 1 – 4 Hz, and a $f_F$ of 20 Hz was better suited for PRFs of 10 – 20 Hz. The key parameters for evaluating the performance of the two cameras were:

- Percentage of Acquired Pulses (%AP) with respect to the total number of laser pulses transmitted in a certain Pulse Train Duration (PTD) for the PHOENIX NIR camera; and
- Real-time Image Quality (RIQ) for the MERLIN NIR camera.

Particularly, for the RIQ the following ranking scale was used in the assessment:

- 0/4 Spot image absent;
- 1/4 Spot image not clear (fading);
- 2/4 Spot image intermittent but clear; and
- 4/4 Spot image continuous and clear.

The final results of the two performance assessments are summarized in Table 7-3.

**Table 7-3: NIR Cameras Tests Results**

| *Laser Parameters* | | | | | | *PHOENIX* | | *MERLIN* | |
|---|---|---|---|---|---|---|---|---|---|
| ***PRF*** | ***PTD*** | ***Energy*** | ***BE*** | ***AF*** | ***$P_D$*** | ***$f_F$*** | ***%AP*** | ***$f_F$*** | ***RIQ*** |
| **1 Hz** | 10 s | 2 μJ | Wide | Yes | 20 ns | 2 Hz | 52% | 10 Hz | 4/4 |
| | 10 s | 2 μJ | Wide | No | 20 ns | 2 Hz | 66% | 10 Hz | 3/4 |
| | 10 s | 2 μJ | Narrow | Yes | 20 ns | 2 Hz | 53% | 10 Hz | 4/4 |
| | 10 s | 2 μJ | Narrow | No | 20 ns | 2 Hz | 67% | 10 Hz | 3/4 |
| **4 Hz** | 10 s | 2 μJ | Wide | Yes | 20 ns | 8 Hz | 47% | 10 Hz | 4/4 |
| | 10 s | 2 μJ | Wide | No | 20 ns | 8 Hz | 66% | 10 Hz | 3/4 |
| | 10 s | 2 μJ | Narrow | Yes | 20 ns | 8 Hz | 48% | 10 Hz | 4/4 |
| | 10 s | 2 μJ | Narrow | No | 20 ns | 8 Hz | 62% | 10 Hz | 4/4 |
| **10 Hz** | 10 s | 2 μJ | Wide | Yes | 20 ns | 20 Hz | 66% | 20 Hz | 3/4 |
| | 10 s | 2 μJ | Wide | No | 20 ns | 20 Hz | 56% | 20 Hz | 3/4 |
| | 10 s | 2 μJ | Narrow | Yes | 20 ns | 20 Hz | 62% | 20 Hz | 4/4 |
| | 10 s | 2 μJ | Narrow | No | 20 ns | 20 Hz | 51% | 20 Hz | 3/4 |
| **20 Hz** | 10 s | 2 μJ | Wide | Yes | 20 ns | 40 Hz | 43% | 20 Hz | 3/4 |
| | 10 s | 2 μJ | Wide | No | 20 ns | 40 Hz | 65% | 20 Hz | 4/4 |
| | 10 s | 2 μJ | Narrow | Yes | 20 ns | 40 Hz | 52% | 20 Hz | 4/4 |
| | 10 s | 2 μJ | Narrow | No | 20 ns | 40 Hz | 48% | 20 Hz | 4/4 |

### 7.5.2 Modified RALM-01 System Testing

This test activity was performed in order to assess the Modified RALM-01 (M-RALM-01) Laser Warning Receiver (LWR) performance in the presence of laser spots generated by very short laser pulses, with PRFs and energy/power levels compatible to the PILASTER program requirements. Particularly, the Optical Units (OUs) of the system were 'stimulated' with laser pulses of low energy levels ($E_t \leq 0.1$ nJ) and power densities ($D_P \leq 5$ mW/m$^2$). The instrumentation arrangement used for the experiment is shown in Figure 7-26.

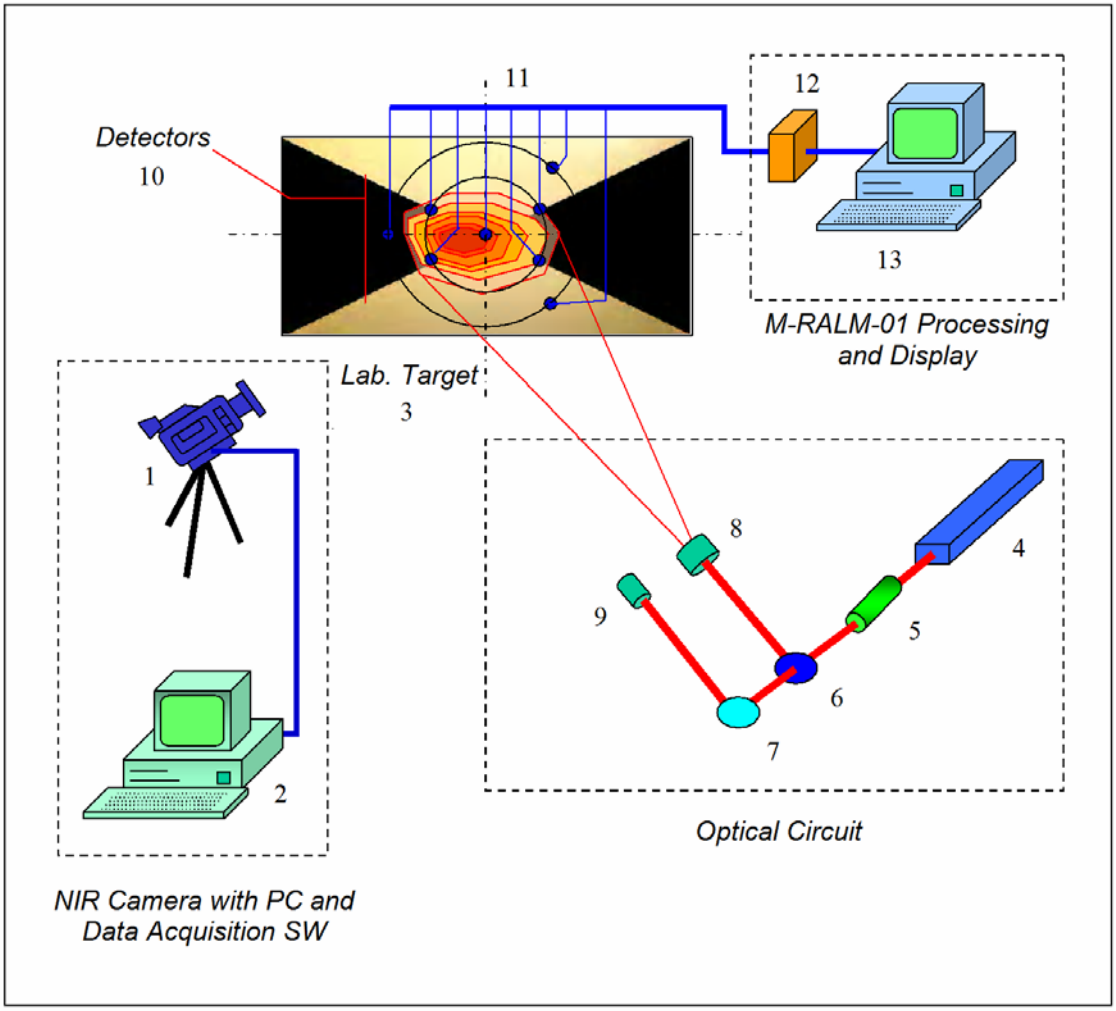


**Figure 7-26: RALM-01 Test Instrumentation Setup.**

Particularly, the following equipment was used in the experiment:

- PHOENIX NIR Camera (1);
- PC based Data Acquisition Systems (2) with IMAGE-PRO PLUS 4.1 software;
- Laboratory Target 3.0 × 1.5 m (3);
- Q-Switched Nd:YAG laser (4);
- Nd:YAG Attenuation Filters (5);
- Beam Splitter (6) and Mirror (7);

- Beam Expanding Optics for Narrow (8) and Wide Laser Beams (9);
- M-RALM-01 Optical Units (10) and Optical Fibre (OF) Cables (11);
- M-RALM-01 Processing Units (12); and
- PC based Data Recording and Display System (13).

The MARCONI LWR Optical Units (OUs) family is shown in Figure 7-27, with evidenced the type of OU used for the M-RALM-01 test (a total number of 8 OU were used for the M-RALM-01 test).

**Figure 7-27: MARCONI LWR OU Family and M-RALM-01 Test OU.**

For comparison purposes, the M-RALM-01 system was also tested without OU, using 'shielded' OF terminations, as shown in Figure 7-28, in order to get a maximum angle of acceptance of ± 20° in accordance with the OF specifications. The PHOENIX NIR camera was also used in the experiment, in order to measure the effective laser spot diameter on the target surface.

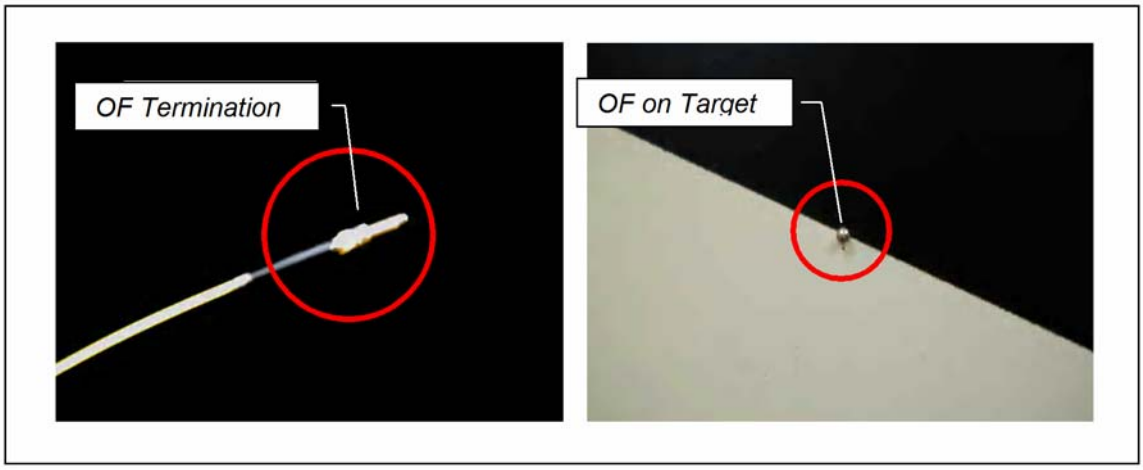


**Figure 7-28: Optical Fibres Shielded Termination.**

The M-RAM-01 Processing Unit, together with an example of the PC based display software format is shown in Figure 7-29.

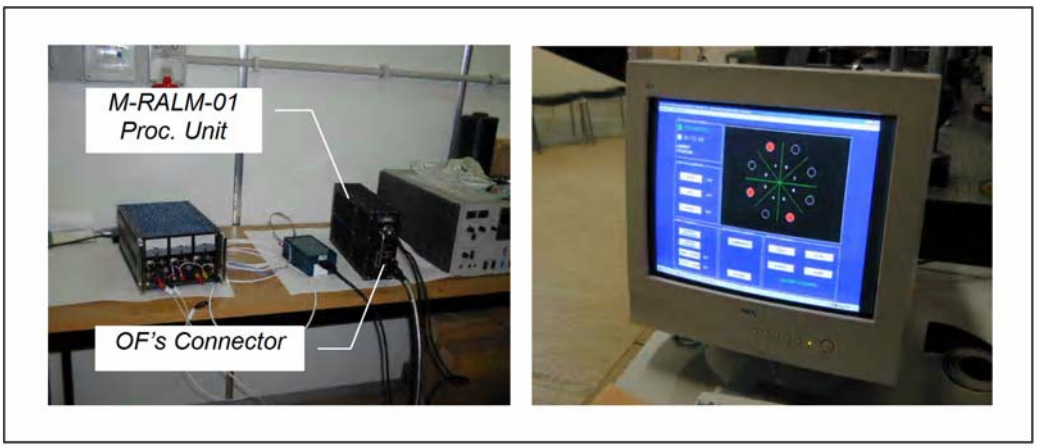


**Figure 7-29: M-RALM-01 MARCONI LWR Processing Unit and PC Display Software.**

In all cases, the M-RALM-01 was capable of detecting the presence of the laser spots, even when the associated pulses peak energies were of the same order of magnitude of the background noise (and the other available instrumentation was not able to detect the laser spots). Furthermore, it was verified that using the OU the directional discrimination capability was substantially increased with respect to the case of 'shielded' OF without OU. Particularly, using very narrow laser spots (i.e., few millimetres), it was observed an acceptance angle of ±5° using the OU, against an effective acceptance angle of ±26° using the 'shielded' OF. However, it was verified that, in both cases, the angular discrimination capability of the system, in the presence of larger laser spots (i.e., 10 – 100 cm) was seriously affected by undesired multiple reflections of the laser spots (i.e., multipath). The conclusion was that, although suitable for detecting the presence of extremely low energy laser pulses and for determining the PRF of incident laser sources, the M-RALM-01 system was not suitable for the laser spot energy measurements required for the PILASTER STU. Therefore, it was decided to use the M-RALM-01 system only as an additional sensor for confirming the presence of laser spots on the PILASTER FXDT target (or in its vicinity) for safety purposes and measuring the PRF of incident laser sources, during both test and training missions.

### 7.5.3 Laser Energy Meter and Detectors Testing

As described in Chapter 5, the PILASTER EMT-1 technique was based on direct energy measurements performed at specific locations on the permanent target, and use of the NIR camera grey-scale PIM to reconstruct the spot energy profile. This concept presented several difficulties for its practical implementation. In fact, it was difficult to find off-the-shelf detectors with sufficiently low NEP characteristics, capable of measuring NIR laser energy from pulses of very low duration (i.e., $P_D$ = 20 nsec) and energy levels ranging from the nJ to the mJ.

After an extensive market survey, and various preliminary laboratory experiments, the best candidate for the PILASTER EMT-1 application (i.e., direct energy measurements at the target location) was the ORIEL 70834 Laser Energy Meter (LEM), equipped with the ORIEL 708XX Pyroelectric Probes (PEP). Some relevant information about the ORIEL 708XX Pyroelectric Probes (PEP) family is reported in Table 7-4.

**Table 7-4: PEP Sensors Characteristics**

| PEP Size (mm) | Max. PD (μs) | Max. Pulse Energy | | Max. PRF (Hz) | Max. Avg. Power (W) | Typical Voltage Resp. ($VmJ^{-1}$) | Noise Equivalent Energy | Model No. |
|---|---|---|---|---|---|---|---|---|
| | | @ 10 ns | @ 1 μs | | | | | |
| 5 | 50 | 1 mJ | 1 mJ | 400 | 2 | 3 | 15 nJ | 70810 |
| 9 | 100 | 4 mJ | 4 mJ | 200 | 2 | 0.8 | 35 nJ | 70811 |
| 25 | 200 | 150 mJ | 1250 mJ | 100 | 5 | 0.008 | 4 μJ | 70825 |
| 50 | 400 | 600 mJ | 5000 mJ | 50 | 10 | 0.002 | 50 μJ | 70827 |

The aim of this test was to verify the performance of the ORIEL 70834 Laser Energy Meter (LEM), equipped with the ORIEL 708XX Pyroelectric Probes (PEP), in terms of data accuracy obtainable using trains of laser pulses with PRF = 10 Hz, very short durations ($P_D$ = 20 nsec) and various energy levels (ranging from the μJ to the hundreds of mJ).

The experiment was carried out using the test setup shown in Figure 7-30, which included the following instrumentation:

- Q-Switched Nd:YAG laser (1);
- Nd:YAG Attenuation Filters (2);
- Narrow band (1064 nm) Filter (3);
- LEM (5) and PEP sensors Under Test (4);
- Oscilloscope (6); and
- PC with Software for Data Display, Analysis and Recording (7).

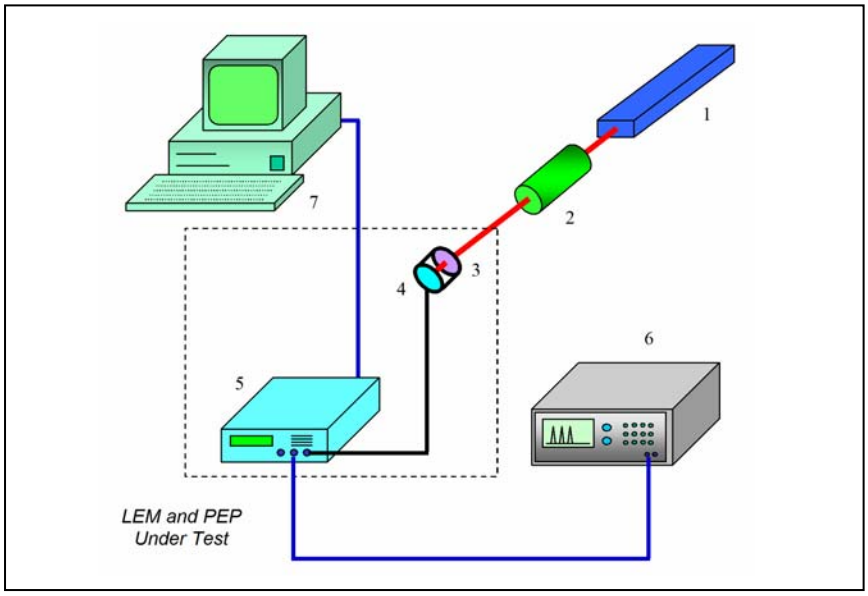


**Figure 7-30: PEP/LEM Initial Test Setup.**

The test was performed with different values of the Laser Output Energy (LOE), a PRF of 10 Hz and a PTD of 5 sec.

The results of the tests performed are reported in Table 7-5. Particularly, the differences (average of 50 measurements and relative standard deviation) between the PEP-LEM readings and the LOE values ($\Delta\%_{PEP\text{-}LOE}$), are listed in the table.

**Table 7-5: PEP/LEM Initial Test Results**

| Laser Parameters | | | | | $\Delta\%_{PEP\text{-}LOE}$* | |
|---|---|---|---|---|---|---|
| PEP | PRF | PTD | LOE | PD | $\mu_{PEP\text{-}LOE}$ | $\sigma_{PEP\text{-}LOE}$ |
| 70810 | 10 Hz | 5 s | 2 μJ | 20 ns | 2.876% | 1.647% |
| | | 5 s | 20 μJ | 20 ns | 1.060% | 1.072% |
| | | 5 s | 200 μJ | 20 ns | -1.120% | 2.283% |
| 70811 | | 5 s | 200 μJ | 20 ns | 3.764% | 1.760% |
| | | 5 s | 2 mJ | 20 ns | -3.022% | 1.445% |
| 70825 | | 5 s | 2 mJ | 20 ns | -2.120% | 1.836% |
| | | 5 s | 20 mJ | 20 ns | -2.334% | 1.945% |
| 70827 | | 5 s | 20 mJ | 20 ns | -4.045% | 2.240% |
| | | 5 s | 200 mJ | 20 ns | 3.908% | 1.808% |

* From 50 PEP measurements.

### 7.5.4 PHOENIX NIR Camera Calibration

Definition of a reliable calibration procedure for the PHOENIX NIR camera was very important for the PILASTER program. Particularly, calibration was required in order to convert the 'grey scale' numeric information associated with the acquired laser spot images (Grey-scale Pixel Intensity Matrix – PIM), into a value of incident energy (integrated in the spectral band of the camera). For this purpose, an Integrating Sphere was used (Figure 7-31). Particularly, with reference to Figure 7-31, the following instrumentation setup was used for the NIR camera calibration:

- PHOENIX NIR Camera (1);
- PC based Data Acquisition Systems (2) with IMAGE-PRO PLUS 4.1 software;
- Q-Switched Nd:YAG laser (3);
- Nd:YAG Attenuation Filters (4);

- Beam Steering Optics (5); and
- Integrating Sphere (6).

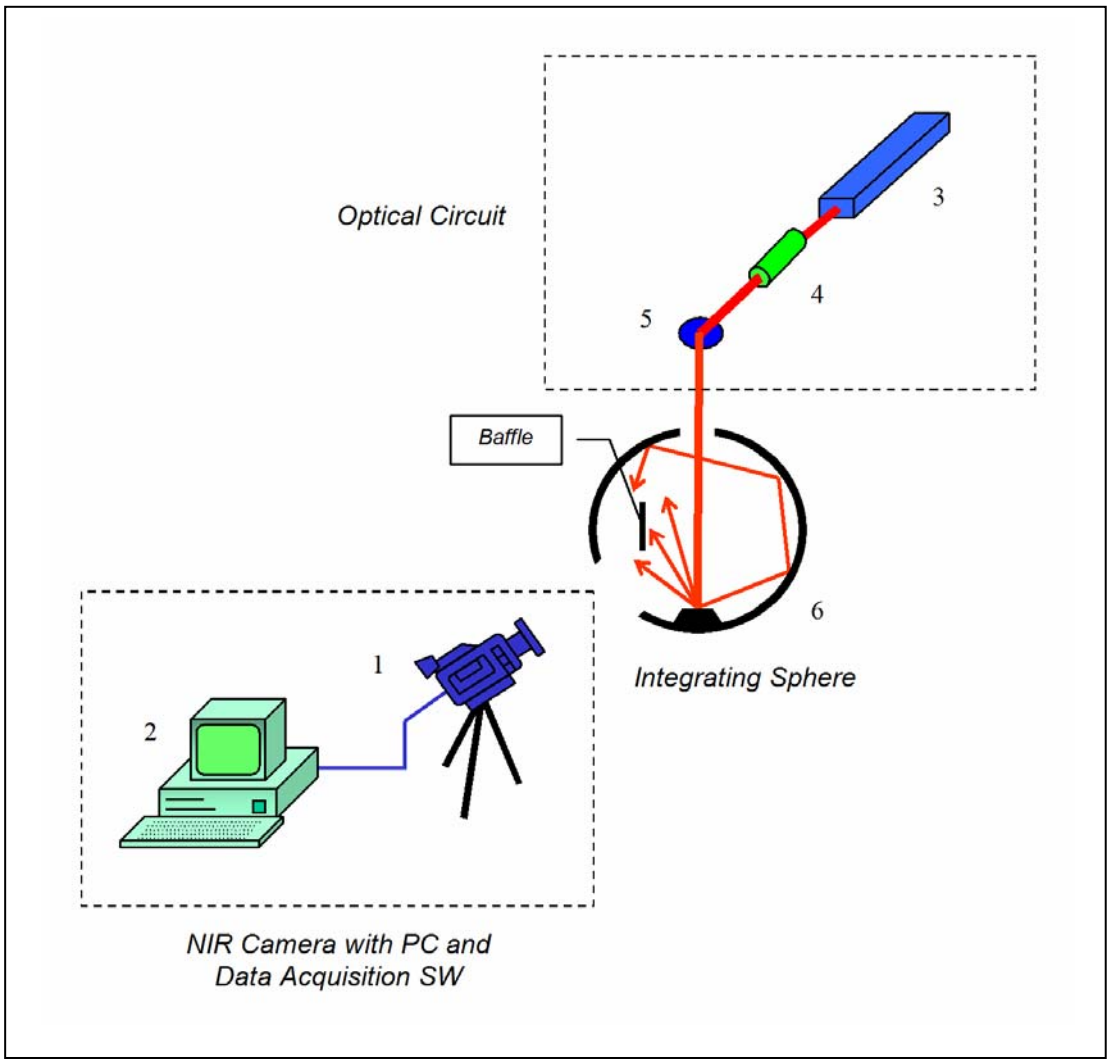


**Figure 7-31: NIR Camera Calibration Procedure.**

IR cameras employing photo-detectors are characterized by an output signal proportional to the incident IR energy. Particularly, in a NIR camera employing a bi-dimensional sensor matrix (i.e., Focal Plane Array – FPA) this is true for every single pixel. Therefore, from the numeric information associated to the image (i.e., Grey-scale Pixel Intensity Matrix – GPIM) it is possible to reconstruct the bi-dimensional map of the energy irradiated by a target within the scene observed by the NIR camera (integrated radiance in the camera spectral band).

In the PHOENIX NIR camera, the FPA analog signals are processed by the read-out electronic circuits, producing a digital output of the image (i.e., 12-bit Analog Digital Unit – ADU). Therefore, constructing a calibration curve for the Radiant Intensities ($W/cm^2sr$) associated to the ADU Grey-scale values, and using a dedicated image analysis software (i.e., IMAGE-PRO PLUS 4.1), it is possible to obtain the image Energy Pixel Intensity Matrix (EPIM) giving the energy associated to each pixel in the NIR camera image.

The linearity of the photo-detector response allows accurate measurements in the camera dynamic range, with only a limited number of calibration data points. Furthermore, NIR cameras like the PHOENIX, featuring a variable integration time (selectable by the operator), give the opportunity of performing measurements in a linear regime within a wide interval of integrated radiance values, thus obtaining reliable measurements.

Calibration of the PHOENIX camera can then be defined as the experimental procedure that allows determination of the ADU/Integrated Radiance Response Function (AIRF). The inverse of the AIRF is used by the image analysis software tool in order to obtain, directly as an image attribute, the values of integrated energy in the spectral band of the camera.

In the case of a photo-detector the response of a single pixel in terms of Analog Digital Unit (ADU) is:

$$ADU_{i,j} \propto \frac{A}{4 \cdot f\#^2 + 1} \cdot g \cdot i_{time} \cdot \int_{\lambda 1}^{\lambda 2} \tau_\lambda \eta \cdot E_\lambda d\lambda \tag{7.4}$$

where $\lambda$ is wavelength, $\lambda_1$ and $\lambda_2$ are the limits of the camera spectral band (with filter), $\eta_\lambda$ is the detector quantum efficiency (whose spectral distribution is typically constant), $E_\lambda$ is the spectral radiance, $\tau_\lambda$ is the optics transmittance, $A$ is the pixel area (30 µm x 30 µm for the PHOENIX-NIR camera), $g$ is the gain of the read-out electronics, $f\#$ is the f-number of the optics and $i_{time}$ is the camera integration time.

Therefore, the experimental parameters to be controlled during the calibration procedure are the integration time, the optics *f*-number and other settings of the NIR camera (e.g., the gain of the read-out electronics which may be selected by the operator). Fixing these parameters for a certain interval of integral radiance, it is possible to determine the AIRF of the camera by using an extended reference source. The function (calibration curve) so obtained, valid for the specific setup of the camera previously defined, is then used to determine the values of integral radiance to be used for reconstructing the radiant intensity map of the target. The spectral response (determined experimentally) of the InGaAs sensor employed in the PHOENIX NIR camera is shown in Figure 7-32.

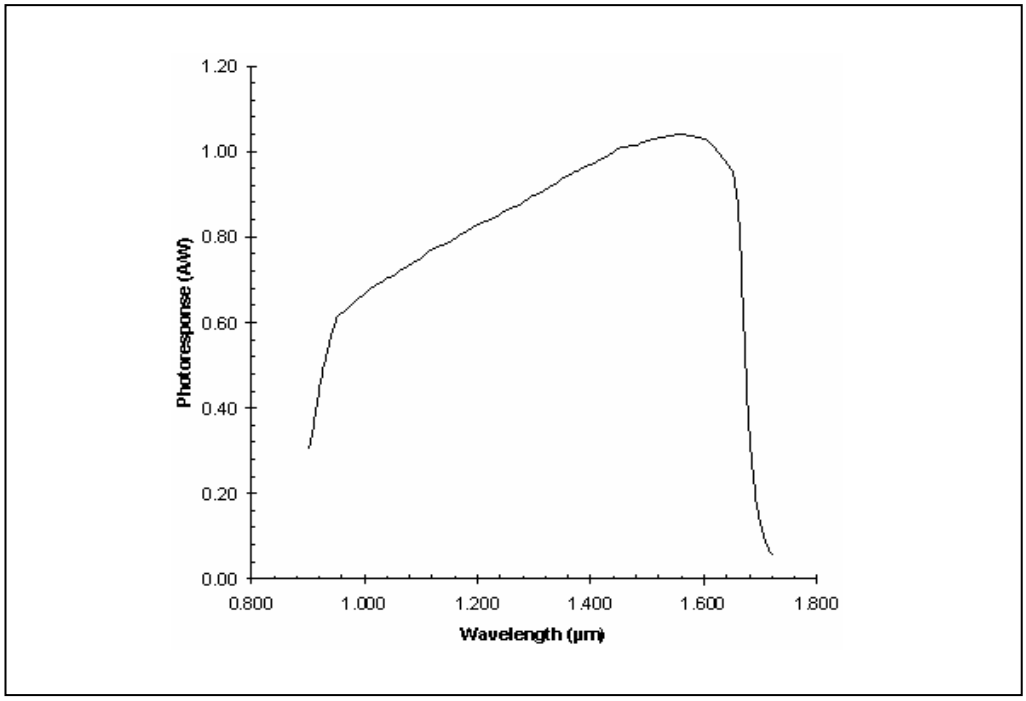


**Figure 7-32: Spectral Response of the FPA Employed in the PHOENIX NIR Camera.**

The curve shows that the sensor output is a value of radiance integrated in the band 0.9 – 1.6 µm. This implies that, in order to perform measurements of the energy reflected by a target (with known reflectance characteristics) illuminated by a laser, it is necessary to considerably reduce the spectral response of the camera by using a narrow band filter (centred at 1064 nm), in order to drastically reduce the contributions of the background. The use of such a filter allows, using the same camera setup, accurate measurements of laser energy, independently from the ambient illumination, both in day and night conditions.

The required calibration source has to be characterised by known (tuneable) energy intensity over an extended area. The ideal match to such requirement is to use an Integrating Sphere with an input from an external variable power reference laser. This is because the Integrating Sphere characteristics are such that it can produce an output uniform energy distribution by using a narrow beamwidth laser as an input.

The steps required to accomplish the NIR camera calibration procedure are the following:

- Define the camera setup parameters (i.e., integration time, f-number of the optics and read-out).
- Set a value $P_1$ of the output power of the laser.
- Obtain the first data point ($P_1$, $ADU_1$), acquiring the camera image and determining the corresponding ADU value ($ADU_1$) using the image analysis and processing tool.
- Modify the laser output power (value $P_2$) and repeat the step 3 in order to determine the second data point ($P_2$, $ADU_2$).
- Repeat the step 4 a number of times sufficient to obtain a stable AIRF solution as the output of a linear interpolation process using all data points ($P_n$, $ADU_n$).
- Repeat the Steps 1 – 5 as required to obtain an AIRF for each combination of camera setup parameters needed operationally.

Using these AIRF with suitable software routines in the image analysis and processing tool, allows obtaining directly on the NIR camera images the relative values of integrated radiance.

## 7.6 LOAS LASER SUB-SYSTEM TESTING

Before performing ground and flight test activities using the LOAS laser system, its $Er^{++}$ doped fibre laser sub-system (IRE POLUS Group mod. ELPM-20K) was tested in the laboratory, in order to determine, against the manufacturer specification documents, the following characteristics:

- Average power transmitted;
- Pulse duration;
- Pulse Repetition Frequency (PRF);
- Laser beam misalignment with respect to the beam-expander support; and
- Power consumption, Weight and Dimensions.

The ELPM-20K laser is shown in Figure 7-33. The instrumentation used for the tests is the following:

- Tester *Hewlett Packard* 3478A;
- Surface Absorption Disk Calorimeter *Scientech* 36-0001;
- Micrometric Support;
- Multimode Optical adapter SMA-FC-PC;
- He-Ne Laser *Melles Griot* 05-LHR-991;

- Oscilloscope *Tektronix* 520D;
- Optical probe *Tektronix* P6703B;
- Optical probe *Tektronix* P6701B;
- Power Supply *Delta* 7020; and
- ND Optical Filters.

**Figure 7-33: ELPM-20K Laser (LOAS).**

The test setup is shown in Figure 7-34. All the measurements were performed in a temperature interval of 18 ÷ 22°C.

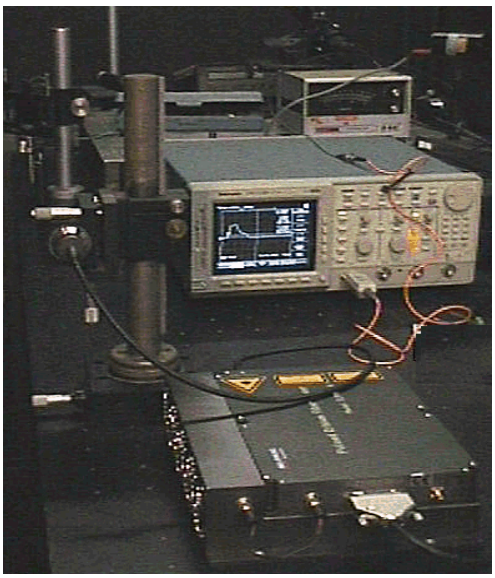

**Figure 7-34: ELPM-20K Test Setup.**

### 7.6.1 Average Power Transmitted

For measuring the average optical power of the laser the disk calorimeter readout has been used, adopting the following procedure:

- Beam expander-calorimeter alignment;
- Laser activation;
- Regulation of the beam direction in order to obtain the maximum readout value on the calorimeter;
- Wait for laser stabilization (20 minutes); and
- Calorimeter readout recording.

Although all prescribed calibration procedures were followed, to check the correctness of the measurement, the calorimeter internal calibration resistance was connected to the power supply. Then the power supply was regulated in order to obtain the same readout previously recorded during the laser activation, and the voltage applied to the resistance was measured using the tester. The voltage readout was $V = 7.757$, with a resistance $R = 41\ \Omega$. Using the formula:

$$P = \frac{V^2}{R \cdot C_O} \tag{7.5}$$

where $C_O$ is the calorimeter optical absorption coefficient (whose value is 0.98), the optical power $P$ equates to 1.49 Watt.

### 7.6.2 Pulse Duration

The laser pulse duration was measured using the oscilloscope optical probe (using the multi-mode optical adapter and ND optical filters between the optical fiber and the beam expander to avoid probe saturation). The result is shown in Figure 7-35.

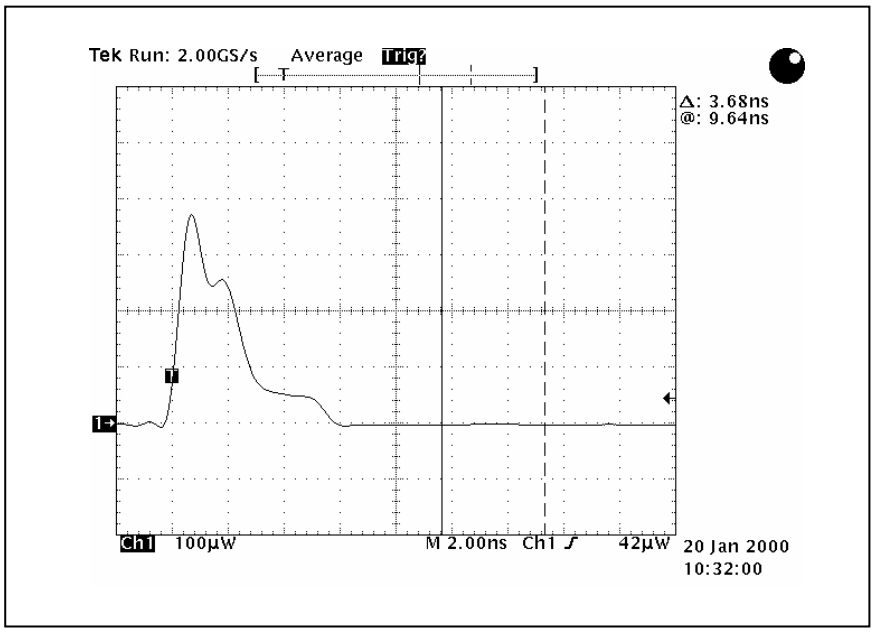


**Figure 7-35: ELPM-20K Pulse Duration Measurement.**

During the measurements, it was noted that there was a marked dependency of the pulse shape on the observation position (probably due to the different modes of propagation of the optical fiber). Therefore, further measurements were performed using the signal reflected by a surface (as in the LOAS real case, where the optical signal received by the APD is reflected from an obstacle).

The result of one of the tests performed using a green painted aluminium target are shown in Figure 7-36. In this situation, an integration of the various optical fiber propagation modes produces a “smooth” pulse shape. This fact is beneficial in terms of the required electrical band for optical-electrical conversion (APD) and signal amplification.

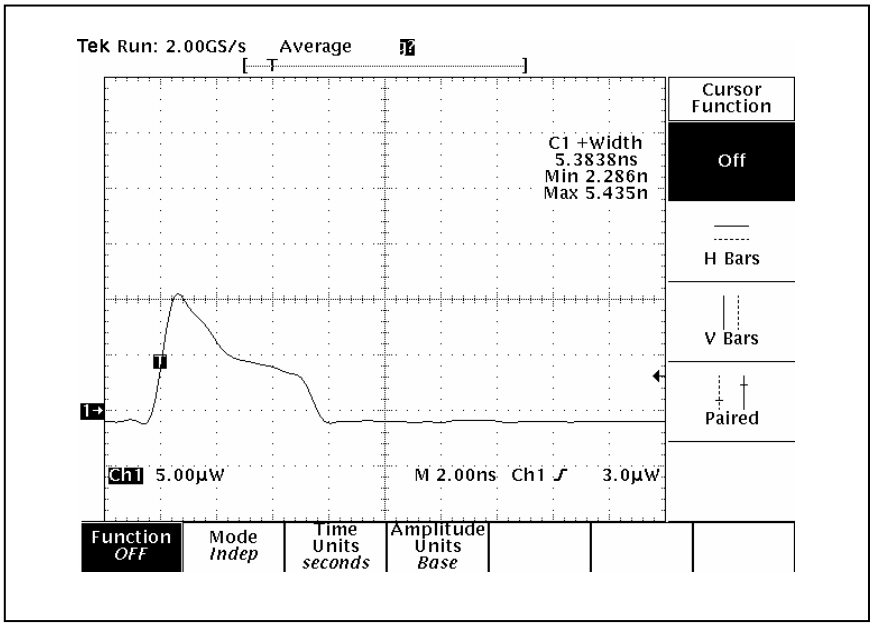


**Figure 7-36: ELPM-20K Pulse Reflected from a Green Painted Target.**

### 7.6.3 Laser Beam Misalignment with Respect to the Beam-Expander Support

For measuring the beam misalignment, the beam expander was placed into the micrometric support, and regulated (azimuth and elevation), in order to obtain a maximum for the signal amplitude measured by the oscilloscope (Figure 7-34). Then the beam expander was replaced by the He-Ne *Melles Griot* laser, whose cylindrical packaging, with the same diameter of the beam expander, is aligned with its laser beam with an error ≤ 1 mrad (small with respect to the alignment error that had to measure: expected value ≤ 10 mrad). Using the probe 6701B (0.5 µm ÷ 0.95 µm band), the micrometric support was regulated in order to obtain a maximum for the amplitude of the signal measured by the oscilloscope. Therefore, measuring the micrometers shifts in azimuth and elevation, the laser beam misalignment was determined. Particularly, the measured misalignment was 5 mrad.

#### 7.6.3.1 Pulse Repetition Frequency

The PRF measurement results (oscilloscope records) are displayed in Figure 7-37.

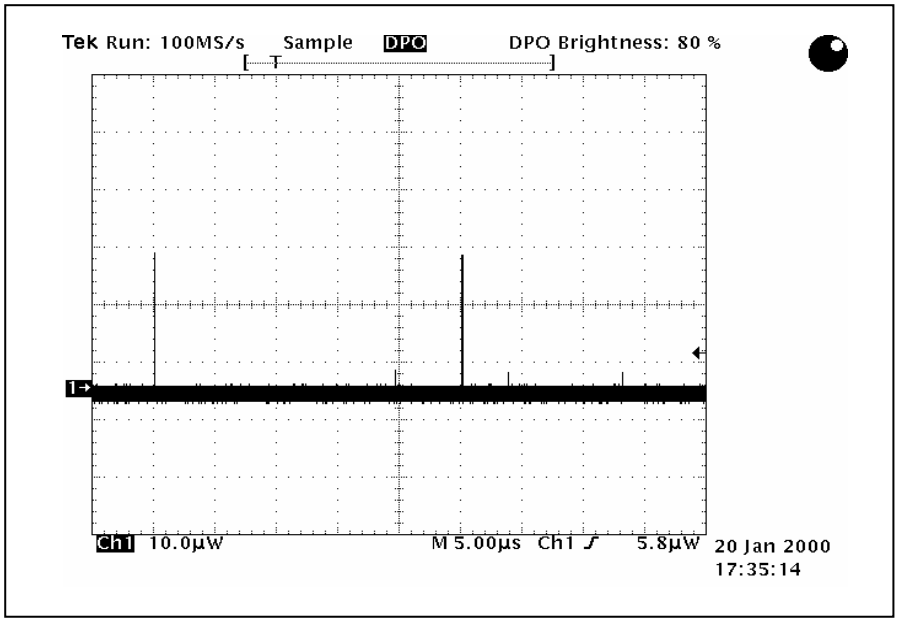


**Figure 7-37: ELPM-20K Pulse Repetition Frequency (PRF).**

#### 7.6.3.2 Power Consumption, Weight and Dimensions

The power consumption measured at 25°C was about 50 W. The need to maintain a constant temperature for the pumping diode (using *Peltier* elements), made power consumption a function of ambient temperature. Tests conducted in a thermal chamber with a temperature range of –10°C ÷ 50°C demonstrated a maximum consumption of 80 W. ELPM-20K laser weight and dimensions were adequate for integration in the LOAS system. The results of all tests performed are summarized in Table 7-6.

**Table 7-6: ELPM-20K Laser Test Results**

| *PARAMETER* | *LOAS SPEC* | *MEASURE* |
|---|---|---|
| Average power transmitted | 1.2 W | 1.49 W |
| Pulse duration | 2 ÷ 5 nsec | 2.8 nsec |
| Pulse Repetition Frequency (PRF) | 40 KHz | 40 KHz |
| Laser beam misalignment with respect to the beam-expander support | 10 mrad | 5 mrad |
| Power consumption | < 200 W | < 50 W @ 25°C |
| Weight | < 4.8 Kg | 3.1 Kg |
| Dimensions | 270 x 50 x 190 mm (LXAXP) | 270 x 35.5 x 190 mm (LXAXP) |

## 7.7 TEST OF PROTECTION FILTERS

During the PILASTER program, a number of laboratory measurements were performed on various protection filters, in order to select the best of current (commercially available) systems (optical density, transmittance in the visible, etc.) for employment at the PILASTER. These measurements included:

- Ground personnel protection goggles;
- Aircrew protection visors and spectacles; and
- LTR Cinetheodolites Operator Sight (COS) filters.

In the last case, the optical gain of the COS needed to be determined first. For all systems, the principal objectives of the laboratory activities were:

- Determination of the filters Optical Density (OD) at $\lambda = 1064$ nm; and
- Determination of the transmittance in the visible.

### 7.7.1 Filters for Ground Personnel and Aircrew

The instrumentation arrangement required to perform the measurements on ground personnel/aircrew protection filters is illustrated in Figure 7-38. With reference to the figure, the following equipment was used:

1) Nd:YAG laser (*Quantel* YG 780-20).
2) Neutral density filters (*Optics for Research* 0.1 ÷ 4.0 ND*)*.
3) Beam-steering optics.
4) Protection filters:
    - *Laser Vision* mod. 01.307.00 (spectacles);
    - *Laser Vision* mod. 01.606.00 (spectacles);
    - *Cilas* mod. IR3-01 (spectacles); and
    - *Gentex* mod. 91A8053-3 (aircrew helmet visor).
5) Lithium tantalite energy detector (*Newport* mod. 818J-50).
6) Multi function optical meter (*Newport* mod. 2835).

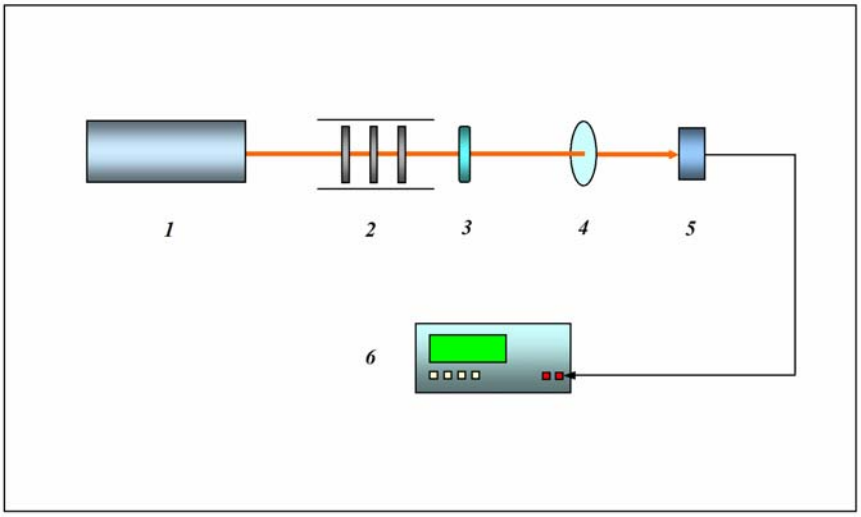


**Figure 7-38: Instrumentation for Filters OD Determination.**

The Optical Densities (OD) of each protection filter was obtained using the average of 5 energy measurements obtained with and without interposition of the protection filter in the optical circuit shown in Figure 7-38, and using the formula:

$$OD = \log_{10} \frac{E_i(H_i)}{E_t(H_t)} \tag{7.6}$$

where $E_i(H_i)$ is the Incident Irradiance (Radiant Exposure) and $E_t(H_t)$ is the Transmitted Irradiance (Radiant Exposure). The various protection filters tested are shown in Figure 7-39.

**Figure 7-39: Tested Laser Protection Filters.**

The results of the measurements are reported in Table 7-7.

**Table 7-7: Protection Filters OD Measurements Results**

| FILTERS | OD | |
|---|---|---|
| | Specified | Measured |
| *Laser Vision* mod. 01.307.00 | 5 | 5.4 |
| *Laser Vision* mod. 01.606.00 | 5 | 5.7 |
| *Cilas* mod. IR3-01 | 4 | 4.6 |
| *Gentex* mod. 91A8053-3 | 3.5 | 3.5 |

Transmission in the visible (*T%*) was measured using the *Perkin Elmer* Lambda-19 spectrometer, equipped with an integrating sphere and capable to determine transmittance in the 350 ÷ 2500 nm spectral range. Before performing the measurements, the instrument was calibrated with a standard $BaSO_4$ reference. For each filter, it was initially performed a scan in the entire instrument spectral range in order to determine the cut-off frequencies, then a fine measurement was performed in the 350 ÷ 750 nm interval. The results of the measurements are presented in Figure 7-40.

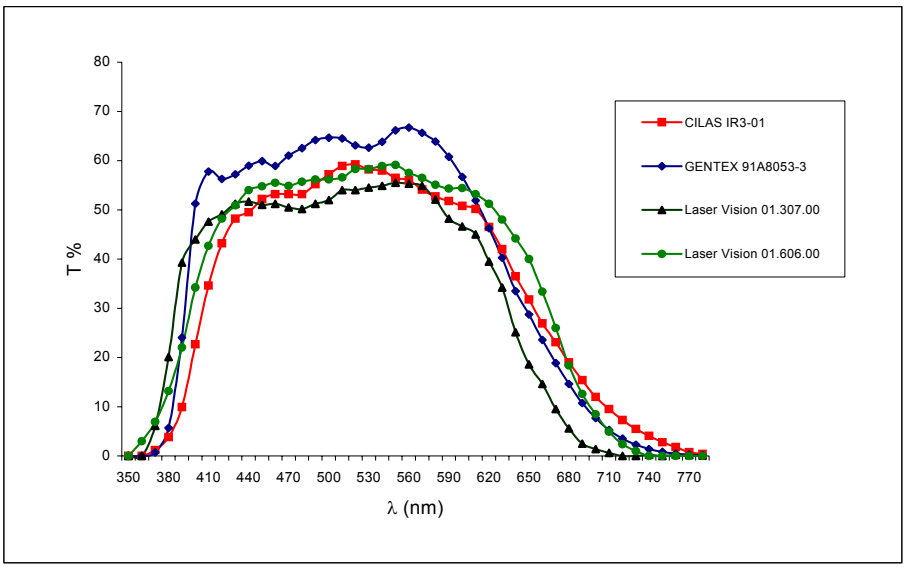


**Figure 7-40: Protection Filters Transmission Measurements Results.**

Although all filters matched the PILASTER program requirements, the filters finally selected were the *Laser Vision* 01.606.00 for ground personnel and the *Gentex* 91A8053-3 visor for aircrews. This last filter, in comparison with other possible laser visors and spectacles, also offered the advantage of an easy integration into the HGU-55/G standard helmet (also produced by *Gentex*) already in service with the Italian Air Force.

### 7.7.2 Test of PILASTER Cinetheodolite Optics

The instrumentation arrangement required to perform the measurements of COS optical gain (*G*) is illustrated in Figure 7-41.

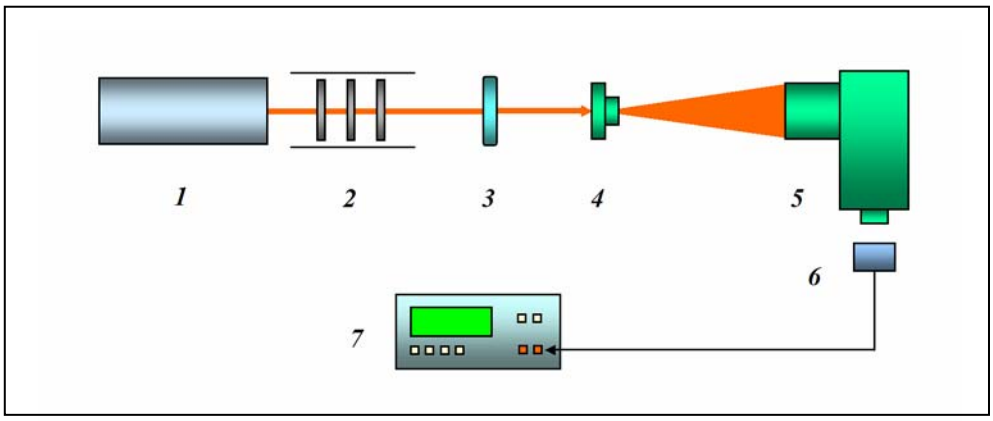


**Figure 7-41: Instrumentation for COS Optical Gain Determination.**

With reference to the figure, the following equipment was used:

1) Nd:YAG laser (*Quantel* YG 780-20);
2) Neutral density filters (*Optics for Research* 0.1÷4.0 ND);

3) Beam-steering optics;
4) Beam expanding optics;
5) PILASTER CITE Operator Sight (*Kern "Solmar"* optics 2× and 12×);
6) Si-photodiode detector (*Newport* low-power detector mod. 818 SL); and
7) Multi function optical meter (*Newport* mod. 2835).

As the COS features two different magnification options ($M$ = 4 and $M$ = 12), the measurements were performed with $M$ = 12 (worst case for safety). The laser irradiance was then measured before the COS input ($E_i$) and successively at the exit pupil of the instrument ($E_o$). The measurements have been performed with different values of input irradiance. The results are reported in Table 7-8, were the values of output laser power ($P_o$) have been normalized (referred to the unit surface).

**Table 7-8: COS Optical Gain Determination**

| Measure | $E_i$ ($\mu$W cm$^{-2}$) | $P_o$ ($\mu$W) | $E_o$ ($\mu$W cm$^{-2}$) | $E_o / E_i = G^2$ | G |
|---|---|---|---|---|---|
| 1 | 1.4 | 18.0 | 143.2 | 102.3 | 10.11 |
| 2 | 2.8 | 36.2 | 288.1 | 102.9 | 10.14 |
| 3 | 8.5 | 108.0 | 859.4 | 101.1 | 10.06 |
| 4 | 26.8 | 344.2 | 2739.1 | 101.5 | 10.07 |
| 5 | 49.2 | 635.3 | 5055.6 | 102.8 | 10.14 |

The optical gain $G$ is required for safety calculations and determination of the appropriate OD for COS operator protection filters. Particularly, given the NOHD of the system to be used at the PILASTER range, the Extended Nominal Ocular Hazard Distance (ENOHD) is given by:

$$ENOHD = NOHD \cdot G + \frac{a \cdot (G-1)}{\phi} \tag{7.7}$$

The OD of the COS operator protection filter is given by:

$$OD \geq \log_{10} \frac{E_{i,KOS}}{E_{MPE}} \tag{7.8}$$

were $E_{MPE}$ is maximum irradiance permitted for the naked human eye (either for a single pulse or for a train of pulses, depending on system mode of operation) and $E_{i,KOS}$ is the irradiance expected to reach the COS operator eye in the absence of a filter, which is given by:

$$E_{i,KOS} = E_{MPE} \cdot G^{-2} \tag{7.9}$$

From the calculation performed using the ELOP-PLD and CLDP technical data, considering the geometries involved with typical test/training missions, a filter with OD ≥ 5 could be used successfully for COS operator protection. Therefore, the *Laser Vision* 01.606.00 filter, already selected for ground personnel, was also suitable for COS operator protection during ELOP-PLD and CLDP missions at the PILASTER range.